6 **Bentley, D. L. and Rabbits, T. H.,** Human immunoglobulin variable region genes – DNA sequences of two V kappa genes and a pseudogene. *Nature* 1980. **288**: 730–733.

7 **Moir, S., Lapointe, R., Malaspina, A., Ostrowski, M., Cole, C. E., Chun, T. W., Adelsberger, J. *et al.*,** CD40-Mediated induction of CD4 and CXCR4 on B lymphocytes correlates with restricted susceptibility to human immunodeficiency virus type 1 infection: potential role of B lymphocytes as a viral reservoir. *J. Virol.* 1999. **73**: 7972–7980.

8 **Kuritzkes, D. R., Jacobson, J., Powderly, W. G., Godofsky, E., DeJesus, E., Haas, F., Reimann, K. A. *et al.*,** Antiretroviral activity of the anti-CD4 monoclonal antibody TNX-355 in patients infected with HIV type 1. *J. Infect. Dis.* 2004. **189**: 286–291.

9 **Burastero, S. E., Gaffi, D., Lopalco, L., Tambussi, G., Borgonovo, B., De Santis, C., Abecasis, C. *et al.*,** Autoantibodies to CD4 in HIV type 1-exposed seronegative individuals. *AIDS Res. Hum. Retroviruses* 1996. **12**: 273–280.

10 **Boon, L., Holland, B., Gordon, W., Liu, P., Shiau, F., Shanahan, W., Reimann, K. A. and Fung, M.,** Development of anti-CD4 MAb hu5A8 for treatment of HIV-1 infection: preclinical assessment in non-human primates. *Toxicology* 2002. **172**: 191–203.

11 **Shearer, M. H., Timanus, D. K., Benton, P. A., Lee, D. R. and Kennedy, R. C.,** Cross-clade inhibition of human immunodeficiency virus type 1 primary isolates by monoclonal anti-CD4. *J. Infect. Dis.* 1998. **177**: 1727–1729.

12 **Hurez, V., Kaveri, S. V., Mouhoub, A., Dietrich, G., Mani, J. C., Klatzmann, D. and Kazatchkine, M. D.,** Anti-CD4 activity of normal human immunoglobulin G for therapeutic use. (Intravenous immunoglobulin, IVIg). *Ther. Immunol.* 1994. **1**: 269–277.

13 **Bomsel, M., Pastori, C., Tudor, D., Alberti, C., Garcia, S., Ferrari, D., Lazzarin, A. and Lopalco, L.,** Natural mucosal antibodies reactive with first extracellular loop of CCR5 inhibit HIV-1 transport across human epithelial cells. *AIDS* 2007. **21**: 13–22.

14 **Sugden, B. and Mark, W.,** Clonal transformation of adult human leukocytes by Epstein–Barr virus. *J. Virol.* 1977. **23**: 503–508.

15 **Takekoshi, M., Maeda, F., Tachibana, H., Inoko, H., Kato, S., Takakura, I., Kenjyo, T. *et al.*,** Human monoclonal anti-HCMV neutralizing antibody from phage display libraries. *J. Virol. Methods* 1998. **74**: 89–98.

16 **Takekoshi, M., Maeda, F., Nagatsuka, Y., Aotsuka, S., Ono, Y. and Ihara, S.,** Cloning and expression of human anti-tumor necrosis factor-alpha monoclonal antibodies from Epstein–Barr virus transformed oligoclonal libraries. *J. Biochem.* 2001. **130**: 299–303.

17 **Matsuda, F., Ishii, K., Bourvagnet, P., Kuma, K., Hayashida, H., Miyata, T. and Honjo, T.,** The complete nucleotide sequence of the human immunoglobulin heavy chain variable region locus. *J. Exp. Med.* 1998. **188**: 2151–2162.

18 **Huber, C., Schable, K. F., Huber, E., Klein, R., Meindl, A., Thiebe, R., Lamm, R. and Zachau, H. G.,** The V kappa genes of the L regions and the repertoire of V kappa gene sequences in the human germ line. *Eur. J. Immunol.* 1993. **23**: 2868–2875.

19 **Pech, M. and Zachau, H. G.,** Immunoglobulin genes of different subgroups are interdigitated within the VK locus. *Nucleic Acids Res.* 1984. **12**: 9229–9236.

20 **Healey, D., Dianda, L., Moore, J. P., McDougal, J. S., Moore, M. J., Estess, P., Buck, D. *et al.*,** Novel anti-CD4 monoclonal antibodies separate human immunodeficiency virus infection and fusion of CD4+ cells from virus binding. *J. Exp. Med.* 1990. **172**: 1233–1242.

21 **Peterson, A. and Seed, B.,** Genetic analysis of monoclonal antibody and HIV binding sites on the human lymphocyte antigen CD4. *Cell* 1988. **54**: 65–72.

22 **Benkirane, M., Hirn, M., Carriere, D. and Devaux, C.,** Functional epitope analysis of the human CD4 molecule: antibodies that inhibit human immunodeficiency virus type 1 gene expression bind to the immunoglobulin CDR3-like region of CD4. *J. Virol.* 1995. **69**: 6898–6903.

23 **Sattentau, Q. J., Dalgleish, A. G., Weiss, R. A. and Beverley, P. C.,** Epitopes of the CD4 antigen and HIV infection. *Science* 1986. **234**: 1120–1123.

24 **Pal, R., Nair, B. C., Hoke, G. M., Sarngadharan, M. G. and Edidin, M.,** Lateral diffusion of CD4 on the surface of a human neoplastic T-cell line probed with a fluorescent derivative of the envelope glycoprotein (gp120) of human immunodeficiency virus type 1 (HIV-1). *J. Cell. Physiol.*1991. **147**: 326–332.

25 **Finnegan, C. M., Rawat, S. S., Cho, E. H., Guiffre, D. L., Lockett, S., MerrillJr., A. H. and Blumenthal, R.,** Sphingomyelinase restricts the lateral diffusion of CD4 and inhibits human immunodeficiency virus fusion. *J. Virol.* 2007. **81**: 5294–5304.

26 **Rawat, S. S., Zimmerman, C., Johnson, B. T., Cho, E., Lockett, S. J., Blumenthal, R. and Puri, A.,** Restricted lateral mobility of plasma membrane CD4 impairs HIV-1 envelope glycoprotein mediated fusion. *Mol. Membr. Biol.* 2008. **25**: 83–94.

27 **Xavier, R., Brennan, T., Li, Q., McCormack, C. and Seed, B.,** Membrane compartmentation is required for efficient T cell activation. *Immunity* 1998. **8**: 723–732.

28 **Millan, J., Cerny, J., Horejsi, V. and Alonso, M. A.,** CD4 segregates into specific detergent-resistant T-cell membrane microdomains. *Tissue Antigens* 1999. **53**: 33–40.

29 **Nguyen, D. H., Giri, B., Collins, G. and Taub, D. D.,** Dynamic reorganization of chemokine receptors, cholesterol, lipid rafts, and adhesion molecules to sites of CD4 engagement. *Exp. Cell. Res.* 2005. **304**: 559–569.

30 **Maeda, F., Nagatsuka, Y., Ihara, S., Aotsuka, S., Ono, Y., Inoko, H. and Takekoshi, M.,** Bacterial expression of a human recombinant monoclonal antibody fab fragment against hepatitis B surface antigen. *J. Med. Virol.* 1999. **58**: 338–345.

31 **Shimizu, S., Urano, E., Futahashi, Y., Miyauchi, K., Isogai, M., Matsuda, Z., Nohtomi, K. *et al.*,** Inhibiting lentiviral replication by HEXIM1, a cellular negative regulator of the CDK9/cyclin T complex. *AIDS* 2007. **21**: 575–582.

32 **Nagatsuka, Y., Hara-Yokoyama, M., Kasama, T., Takekoshi, M., Maeda, F., Ihara, S., Fujiwara, S. *et al.*,** Carbohydrate-dependent signaling from the phosphatidylglucoside-based microdomain induces granulocytic differentiation of HL60 cells. *Proc. Natl. Acad. Sci. USA* 2003. **100**: 7454–7459.

Abbreviations: **B-LCL:** B-lymphoblastoid cell lines · **rhCD4:** recombinant human CD4 · **SHM:** somatic hypermutation

Full correspondence: Dr. Jun Komano, AIDS Research Center, National Institute of Infectious Diseases, 1-23-1 Shinjuku, Tokyo 162-864, Japan
Fax: +81-3-5285-1111
e-mail: ajkomano@nih.go.jp

Additional correspondence: Dr. Masataka Takekoshi, Department of Molecular Life Science, Division of Basic Molecular Science and Molecular Medicine, Tokai University School of Medicine, Isehara, Japan
e-mail: mtakekos@is.icc.u-tokai.ac.jp

Received: 2/4/2009
Revised: 22/12/2009
Accepted: 1/2/2010
Accepted article online: 16/2/2010

Cancer Science
The official journal of the Japanese Cancer Association JCA

Dominant-negative derivative of EBNA1 represses EBNA1-mediated transforming gene expression during the acute phase of Epstein–Barr virus infection independent of rapid loss of viral genome

Yumi Kariya,[1,2] Makiko Hamatake,[1] Emiko Urano,[1] Hironori Yoshiyama,[3] Norio Shimizu[2] and Jun Komano[1,4]

[1]AIDS Research Center, National Institute of Infectious Diseases, Tokyo; [2]Department of Virology, Division of Medical Science, Medical Research Institute, Tokyo Medical and Dental University, Tokyo; [3]Research Center for Infection-associated Cancer, Institute for Genetic Medicine, Hokkaido University, Sapporo, Japan

(Received November 1, 2009/Revised November 30, 2009/Accepted December 6, 2009/Online publication February 2, 2010)

The oncogenic human herpes virus, the Epstein–Barr virus (EBV), expresses EBNA1 in almost all forms of viral latency. EBNA1 plays a major role in the maintenance of the viral genome and in the transactivation of viral transforming genes, including EBNA2 and latent membrane protein (LMP-1). However, it is unknown whether inhibition of EBNA1 from the onset of EBV infection disrupts the establishment of EBV's latency and transactivation of the viral oncogenes. To address this, we measured EBV infection kinetics in the B cell lines BALL-1 and BJAB, which stably express a dominant-negative EBNA1 (dnE1) fused to green fluorescent protein (GFP). The EBV genome was surprisingly unstable 1 week post-infection: the average loss rate of EBV DNA from GFP- and GFP-dnE1-expressing cells was 53.4% and 41.0% per cell generation, respectively, which was substantially higher than that of an 'established' *oriP* replicon (2–4%). GFP-dnE1 did not accelerate loss of the EBV genome, suggesting that EBNA1-dependent licensing of the EBV genome occurs infrequently during the acute phase of EBV infection. In the subacute phase, establishment of EBV latency was completely blocked in GFP-dnE1-expressing cells. In contrast, C/W promoter-driven transcription was strongly restricted in GFP-dnE1-expressing cells at 2 days post-infection. These data suggest that inhibition of EBNA1 from the onset of EBV infection is effective in blocking the positive feedback loop in the transactivation of viral transforming genes, and in eradicating the EBV genome during the subacute phase. Our results suggest that gene transduction of GFP-dnE1 could be a promising therapeutic and prophylactic approach toward EBV-associated malignancies. (*Cancer Sci* 2010; 101: 876–881)

The Epstein–Barr virus (EBV) is a risk factor in several malignant diseases including Burkitt's lymphoma and nasopharyngeal carcinoma.[1–4] The opportunistic B-cell lymphoma is becoming the major cause of death in AIDS patients in an era of highly active antiretroviral therapy (HAART), and EBV is associated with a significant portion of AIDS lymphoma cases.[5,6] Neither an EBV vaccine, nor specific antiviral agents against EBV are available; thus attention should be paid to the development of therapeutic agents against EBV.

EBV-encoded genes including EBNA1, EBNA2, and latent membrane protein (LMP-1) are potential molecular targets for the treatment of EBV-associated lymphomas because they play central roles in the process of malignant transformation.[7] We are interested in EBNA1 since it contributes to EBV oncogenesis in two ways: it supports the maintenance of the EBV genome in *cis* and enhances expression of viral oncogenes, including EBNA2 and LMP-1, in *trans*.[7–9] EBNA1 exerts its biological functions by binding to its cognate binding sites within the family of repeats (FR) and the dyad symmetry element (DS) located within the origin of replication (oriP) of EBV DNA. EBNA1 interacts with FR to enhance transcription from the viral C/W promoters (C/Wp) and to partition EBV DNA to daughter cells; and with DS to initiate DNA replication.[7–9]

Maintenance of the oriP replicon is stable once EBV latency has been established. The loss rate of established oriP plasmids is estimated at 2–4% per cell generation.[10,11] Interestingly, the loss rate of the oriP replicon is significantly higher in cells transiently transduced with oriP plasmids (>25% per cell generation) than in established cells.[12] In primary B cells, EBV DNA is lost rapidly within 2 days post-infection (~98.9%).[13] However, the loss rate of the EBV genome during a week post-infection in B cells remains to be quantified.

Upon EBV infection, the first viral genes expressed are the transactivators EBNA2 and EBNA-LP transcribed from Wp several hours after infection.[7] EBNA2 binds to the EBNA2-responsive elements and, in cooperation with EBNA-LP, enhances transcription from Cp, which leads to expression of all EBNA proteins, including EBNA1. EBNA1 binding to oriP activates C/Wp to boost viral latent gene expression, including the EBNAs and LMP-1. The viral gene transactivation positive feedback loop is established within a few days post-infection, and EBNA1 is one of the key factors that sustain this feedback loop during the acute phase of EBV infection.[14] In parallel, EBNA1 contributes to the establishment of the EBV genome as a licensed replicon. It may be possible to stop EBV infection by breaking the chain of EBNA1-dependent events and thus the EBV-mediated malignant transformation of infected cells. Previous studies have assessed the therapeutic potential of a dominant-negative derivative of EBNA1 (dnE1) in cells in which EBV latency was already established.[15,16] In this study, we critically assessed whether inhibition of EBNA1 limits the early stage of EBV infection in B cells. We provide evidence that expression of dnE1 strongly blocks the expression of virus-encoded oncogenes in acutely infected cells without accelerating EBV genome loss, and disrupts EBV latency in the subacute phase of EBV infection.

Materials and Methods

Cells. The 293T, EBV-negative Burkitt lymphoma cell line BJAB, EBV-positive Burkitt lymphoma cell line Daudi, EBV-transformed healthy donor-derived B lymphoblastoid cell line (B-LCL), and B acute lymphoblastic leukemia cell line BALL-1

[4]To whom correspondence should be addressed.
E-mail: ajkomano@nih.go.jp

doi: 10.1111/j.1349-7006.2009.01474.x

cells (kindly provided by Dr. Yokota, National Institute of Infectious Diseases, Tokyo, Japan) were maintained in RPMI-1640 medium (Sigma, St. Louis, MA, USA) supplemented with 10% fetal bovine serum (Japan Bioserum, Tokyo, Japan), 50 U/mL penicillin, 50 μg/mL streptomycin (Invitrogen, Tokyo, Japan), and incubated at 37°C in a humidified 5% CO_2 atmosphere.

Plasmids. The following primers were used to amplify dnE1 from p1160[17] by PCR: 5′-ACCGGTCTCGAGCAATTGCCA-CCATGCGGGGTCAGGGTGATGGAGG-3′ and 5′-GGATC-CTCGAGCGGCCGCTCACTCCTGCCCTTCCTCACC-3′. The GFP-dnE1 expression vector (pGD) was constructed by cloning the MfeI-XhoI fragment of the PCR product into the BglII-SalI sites of pEGFP-C1 (Clontech, Palo Alto, CA, USA). The MfeI and BglII sites were blunted with T7 RNA polymerase. The AgeI-BamHI fragment from pGD was cloned into the corresponding restriction sites of pCMMP eGFP[15,18] to generate pCMMP GFP-dnE1. The EBNA1 expression vector p1553, the FR-tk-luciferase reporter p985, and pLuciferase (pCMV-luc) have been described previously.[17–20]

Luciferase assay. The 293T cells, grown in 48-well plates, were co-transfected with the indicated plasmids using Lipofectamine 2000 according to the manufacturer's protocol (Invitrogen, Tokyo, Japan). Cells were replated in 96-well plates in triplicate at 2 h post-transfection. Luciferase activity was measured 48 h after transfection using the Steady-Glo Kit (Promega, Madison, WI, USA).

Murine leukemia virus (MLV) vector infection and cell sorting. MLV vectors were produced as described previously.[18] B cells (1×10^7 cells) were incubated with 2 mL of MLV preparation overnight at 4°C with continuous agitation. GFP-positive cells were collected using a FACS sorter (FACS Vantage; Becton Dickinson, San Jose, CA, USA) at 11 days post-infection.

Western blotting. Western blotting was performed as described previously.[21,22] The following reagents were used: anti-GFP (MsX Green Fluorescent Protein; Chemicon, Temecula, CA, USA) and Envision+ Dual Link System-HRP (Dako, Glostrup, Denmark).

EBV infection and nucleic acid extraction. The EBV B95-8 strain was a generous gift from Dr Fujiwara's group at the National Research Institute for Child and Development (Tokyo, Japan). B cells (1×10^7 cells) were incubated with 100 μL of B95-8 EBV for 1 h at 37°C, and genomic DNA was extracted from half of the infected cells soon after infection (QIAamp DNA Mini Kit; Qiagen, Tokyo, Japan). At 15 h post-infection, half of the cells were washed once with PBS and incubated for 5 min in lysis buffer (10 mM Tris-HCl [pH7.4], 10 mM NaCl, 3 mM $MgCl_2$, and 0.5% NP-40). The nuclear fraction was collected by centrifugation for 5 min at 20.6 K × *g* (Kubota 3740; Kubota, Tokyo, Japan), and high molecular weight DNA was extracted (nuclear DNA). At 2 days post-infection and at later time points, high molecular weight DNA, or total RNA (PureLink Total RNA Blood Purification Kit; Invitrogen) was extracted from 1×10^6 or 3×10^6 cells, respectively, according to the manufacturer's protocol. After EBV infection, 10 μM aciclovir (Kayaku, Tokyo, Japan) was added to the culture medium. The production and infection of the recombinant EBV Akata strain carrying GFP and neomycin resistant genes has been described previously.[23] At 2 days post-infection, cells were plated at a density of 1×10^4 cells per well in a flat-bottomed 96-well plate, and cultured in a medium containing 1 mg/mL G418. The efficiency of EBV latency establishment was evaluated as percentage of wells positive for the emergence of G418-resistant cells at 2 to 3 weeks post-G418 selection.

Quantitative real-time PCR. Real-time PCR was performed as described previously; serial dilutions of positive controls were used as standards.[21] Amplifications were performed using the QuantiTect SYBR Green RT-PCR/PCR Kit (Qiagen), and the following primers: BamHI W repeat, 5′-GCCAGAGG-TAAGTGGACTTT-3′ and 5′-AGAAGCATGTATACTAAGC-CTCCC-3′; cyclophilin A (CYPA), 5′-CACCGCCACCATG-GTCAACCCCA-3′ and 5′-CCCGGGCCTCGAGCTTTCGAG-TTGTCCACAGTCAGCAATGG-3′; C/Wp, 5′-CCCTCGGA-CAGCTCCTAAG-3′ and 5′-CTTCACTTCGGTCTCCCCTA-3′; EBER1, 5′-AAAACATGCGGACCACCAGC-3′ and 5′-AG-GACCTACGCTGCCCTAGA-3′. The β-globin primers were described previously.[21] Following PCR amplification, the amplicons were separated in a 2% agarose gel, stained with ethidium bromide, and imaged with a Typhoon scanner (GE Healthcare Bio-Sciences; Piscataway, NJ, USA).

Results

Construction and functional verification of dnE1 fused to GFP. The carboxy half of EBNA1 serves as a functional dominant-negative inhibitor of EBNA1 that restricts the replication and maintenance of oriP plasmids as well as the EBNA1-dependent enhancement of transcription.[17,24] We used a dnE1 mutant encompassing amino acids 377 to 391 (the nuclear localization signal, NLS) and 451 to 641 (the DNA binding and dimerization domain) of EBNA1 (Fig. 1A).[17] To visualize the intracellular distribution of dnE1, we constructed the retroviral expression vector encoding GFP-dnE1. The expression of GFP-dnE1 was verified in transiently transfected 293T cells and stably transduced B cell lines using an MLV vector. To verify the function of GFP-dnE1, we conducted a reporter assay using a plasmid encoding the FR-tk-luciferase cassette. EBNA1 enhances expression of FR-tk-luciferase by binding to FR. If the GFP-dnE1 construct retains dnE1 function, co-expressing EBNA1 and GFP-dnE1 should reduce reporter activity. Luciferase activity was increased significantly upon EBNA1 expression by approximately 5.3-fold, consistent with previous findings (Fig. 1B, $P < 0.05$, two-tailed Student's *t*-test).[17] When GFP-dnE1 was co-expressed, the luciferase activity was decreased. The decrease in luciferase activity was proportional to the increase in GFP-dnE1 expression vector (Fig. 1B, maximum reduction: 22.3%, $P < 0.05$, two-tailed Student's *t*-test). This effect was not observed with GFP alone. In addition, CMV promoter-driven luciferase expression was unaffected by EBNA1, GFP-dnE1, and GFP, suggesting that the reduction in luciferase activity with GFP-dnE1 in the EBNA1/FR-tk-luciferase system is specific. These data indicate that GFP-dnE1 functions as an inhibitor of EBNA1.

Establishment of B cells constitutively expressing GFP-dnE1. To investigate the potential effect of GFP-dnE1 on EBV infection in B cells, we established BALL-1 and BJAB cells, which constitutively express GFP-dnE1, using an MLV vector. GFP was used as a control throughout this study. The distribution of GFP-dnE1 was examined by confocal microscopy, which revealed an even distribution of GFP throughout the cell. In contrast, the majority of GFP-dnE1was localized to the nucleus due to the presence of the NLS (Fig. 2A). Similar observations were made in BJAB and 293T cells (data not shown). We sorted the GFP- or GFP-dnE-expressing cells using a FACS sorter. To test the dose-dependent effect, we collected BALL-1 cell populations bearing high or low levels of GFP fluorescence, denoted as Hi and Lo, respectively. The expression of GFP and GFP-dnE1 was verified by Western blotting, which confirmed that GFP and GFP-dnE1 Hi cells had higher intensity signals than the GFP and GFP-dnE1 Lo cells (Fig. 2B). The rate of cell proliferation and the morphology of GFP-dnE1 cells were indistinguishable from those of GFP cells (Fig. 2A and data not shown).

Effect of GFP-dnE1 on the nuclear translocation of EBV DNA during the acute phase of EBV infection. To assess whether GFP-dnE1 could restrict the nuclear targeting of the EBV

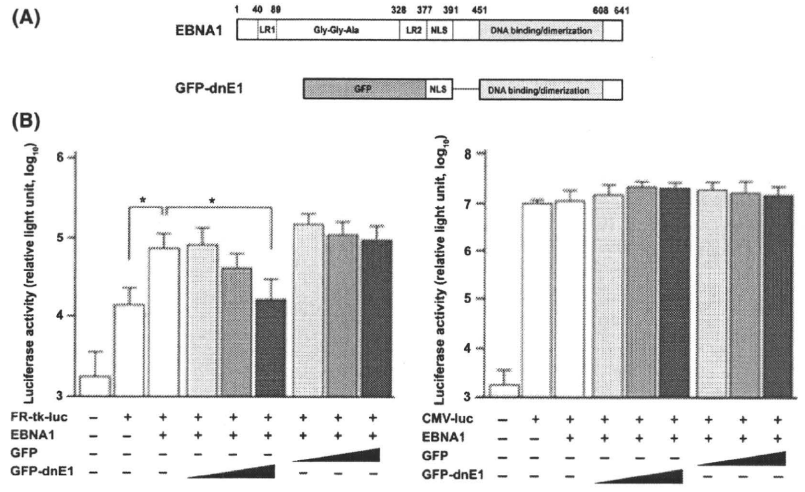

Fig. 1. Construction and functional characterization of a dominant-negative EBNA1 mutant (dnE1) fused to green fluorescent protein (GFP). (A) Structure of the EBNA1 protein and dnE1 used in this study. The linking regions (LR1 and LR2), the Gly-Gly-Ala repeat, the nuclear localization signal (NLS), and the DNA binding and dimerization domain are shown. GFP-dnE1 encodes the NLS and DNA binding and dimerization domain of EBNA1 fused to the C-terminus of GFP. (B) Repression of EBNA1-dependent transcriptional activation by GFP-dnE1. We transfected 293T cells in 48-well plates with 200 ng of FR-tk-luc or CMV-luc reporter, and 500 ng of EBNA1 expression vector, along with increasing amounts of GFP or GFP-dnE1 expression vector (20, 100, and 500 ng, respectively). $*P < 0.05$, two-tailed Student's *t*-test.

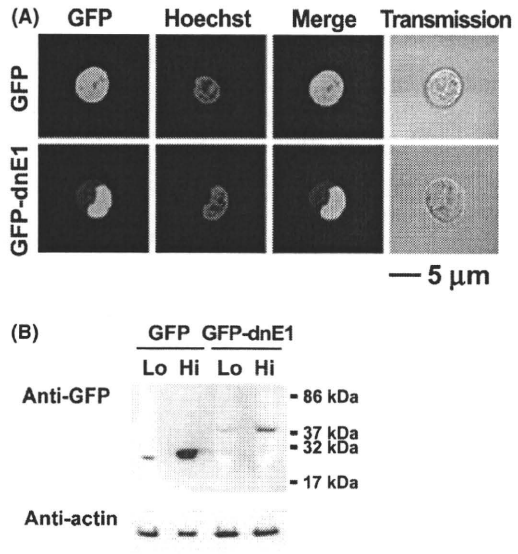

Fig. 2. Verification of stable green fluorescent protein (GFP)-dominant-negative EBNA1 (dnE1) expression in BALL-1 cells. (A) Distribution of GFP and GFP-dnE1 in BALL-1 cells was examined by confocal microscopy. Cells were imaged unfixed using a confocal microscope META 510 (Carl Zeiss, Tokyo, Japan). The green signal represents GFP fluorescence, and blue represents the Hoechst-stained nucleus. The bar represents 5 μm; magnification, ×630. (B) GFP or GFP-dnE1 expression in stably transduced BALL-1 cells was examined by Western blot analysis using an anti-GFP antibody. Protein lysates from 5×10^5 cells were loaded for each sample, except GFP Hi cells (5×10^4). The molecular weight marker is shown on the right.

genome after infection, we measured the amount of EBV DNA recovered from cells immediately after infection (representing the amount of EBV attached to cells) and the amount of EBV DNA that had migrated into the nucleus at 1 day post-infection. We isolated the nuclear fraction to exclude EBV DNA that failed to enter the nucleus. The number of EBV DNA molecules per cell was estimated by real-time PCR, which targeted the BamHI W repeat, in 10 ng of genomic DNA. We estimated the number of EBV DNA per cell given that a single cell contains approximately 10 pg of genomic DNA, and an EBV DNA has 10 copies of BamHI W repeats on average. The nuclear targeting efficiencies of EBV DNA were as follows: BALL-1 GFP cells, 43.3–108.6%; GFP-dnE1 cells, 46.9–65.6%; BJAB GFP cells, 37.4%; GFP-dnE1 cells, 35.0% (Table 1). These data suggested that the effect of GFP-dnE1 on the nuclear targeting of EBV DNA should be assessed more sensitively in BALL-1 and BJAB cell systems than in primary B cells because the nuclear targeting efficiency of EBV DNA in primary B cells is extremely inefficient (~1.1%).[13] In our experimental systems, the nuclear targeting efficiencies of EBV DNA in GFP-dnE1-expressing cells were similar to those in GFP-expressing cells. In addition, the dose-dependency of GFP-dnE1 was not observed in BALL-1 cells (Table 1). These data suggest that the nuclear targeting efficiency of EBV DNA was not restricted by the presence of GFP-dnE1 in B cells upon EBV infection.

Effect of GFP-dnE1 on the rate of loss of EBV DNA during the acute phase of EBV infection. To examine the effect of GFP-dnE1 on the rate of loss (ROL) of EBV DNA during the acute phase of viral infection, we monitored the EBV DNA copy number from day 2 to day 5 or day 6 post-infection, by real-time PCR, which detects the viral genome in both linear and circular configurations (Table 1). The ROL was estimated as the percentage reduction of EBV DNA per cell generation, considering that the cell doubling time is 24 h, and the kinetics of viral genome loss follows an exponential decay. The ROL in GFP-dnE1-expressing cells (19.2–85.9% per cell generation) was similar to GFP-expressing cells (20.5–79.4% per cell generation) in both BALL-1 and BJAB cells. In addition, there was no detectable dose-dependent effect of GFP-dnE1 in BALL-1 cells (Table 1 and Fig. 3). The averages ± SEs of ROL in GFP- and GFP-dnE1-expressing cells from six independent measurements in BALL-1 cells were 37.7 ± 10.7% and 25.7 ± 6.5% per cell generation, respectively (data not shown), which was substantially higher than the rate of loss of an established oriP replicon (2–4%).[10,11] These results reflect the precipitous loss of oriP plas-

doi: 10.1111/j.1349-7006.2009.01474.x

Table 1. The kinetics of EBV DNA in the acute phase of EBV infection

Cell	Copy number of EBV DNA per cell at the indicated day†				Nuclear transport (%‡)	Rate of loss of EBV DNA (% per cell generation§)
Expt 1						
BALL-1	Day 0	Day 1	Day 2	Day 5		
GFP Hi	20.38	11.92	3.57	0.01¶	58.5	85.9
GFP Lo	17.26	11.68	3.21	0.56	67.7	44.1
GFP-dnE1 Hi	23.02	10.79	3.30	0.30	46.9	54.9
GFP-dnE1 Lo	18.83	12.36	1.46	0.53	65.6	28.7
BJAB	Day 0	Day 1	Day 2	Day 5		
GFP	155.1	58.8	5.38	0.06	37.4	77.7
GFP-dnE1	64.6	37.4	5.69	0.05	58.0	79.4
Expt 2						
BALL-1	Day 0	Day 1	Day 2	Day 6		
GFP Hi	16.33	17.73	11.10	4.74	108.6	19.2
GFP Lo	17.35	7.51	8.75	1.13	43.3	40.1
GFP-dnE1 Hi	18.46	8.71	8.95	3.38	47.2	21.6
GFP-dnE1 Lo	14.14	7.05	6.97	2.79	49.9	20.5

†Nuclear DNA was used for day 1 data. ‡Estimated from day 0 and day 1 data. §Estimated from day 2 and day 5 or day 6 data with the exponential decay. ¶Below the limit of detection. dnE1, dominant-negative EBNA1; EBV, Epstein–Barr virus; GFP, green fluorescent protein.

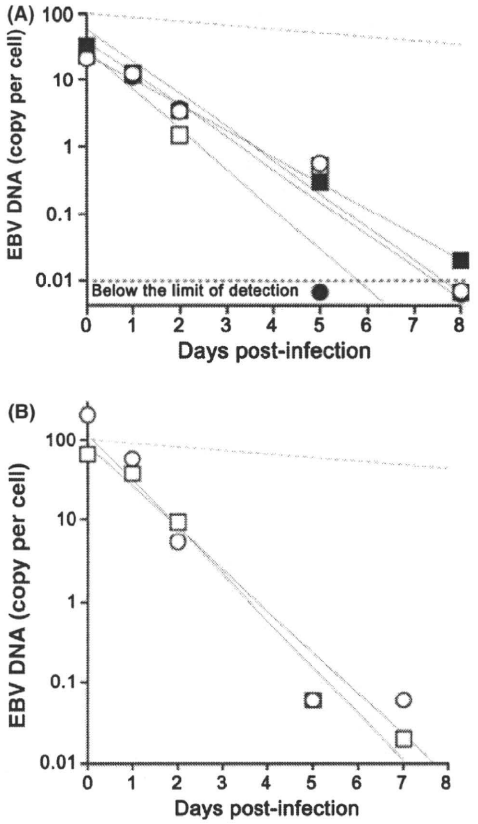

Fig. 3. Kinetics of Epstein–Barr virus (EBV) DNA loss during the acute phase of EBV infection. (A) Representative data from BALL-1 cells (Expt. 1 in Table 1) is shown. The filled squares, open squares, filled circles, and open circles represent GFP Hi, GFP Lo, GFP-dnE1 Hi, and GFP-dnE1 Lo, respectively. The limit of detection was below 0.01 (dashed line). The gray lines represent an approximation to the exponential decay. The dashed gray line represents the 4% rate of loss per cell generation. (B) Representative data from BJAB cells shown in Table 1. The circles and squares represent GFP and GFP-dnE1, respectively. Please see Table 1 for the detailed analysis.

mids (26–37%) in transiently transfected non-B cells.[12] The data suggest that GFP-dnE1 is unable to accelerate the ROL in the acute phase of EBV infection in B cells, presumably because the EBV genome is not established as an EBNA1-dependent stable licensed replicon. It should be noted that this is the first time that quantitative ROL data has been obtained by introducing the oriP replicon into B cells via EBV infection, which is an approach that does not confer any selective advantage on the infected cells.

Effect of GFP-dnE1 on efficiency of establishment of EBV latency. Cells infected with recombinant EBV, carrying the neomycin resistance gene, were seeded at 5×10^3 cells per well into a 96-well plate, and the efficiency of the establishment of EBV latency was assessed as the percentage of wells positive for the emergence of G418-resistant cells. G418-resistant cells appeared in BJAB, Daudi, parental BALL-1, and BALL-1 GFP cells at 56–100% efficiencies. In sharp contrast, G418-resistant cells were absent from GFP-dnE1-expressing BALL-1 cells (Table 2). These data clearly suggest that, although the ROL during the acute phase of EBV infection was not enhanced by GFP-dnE1, GFP-dnE1 was able to block the establishment of EBV latency completely during the subacute phase of EBV infection.

Effect of GFP-dnE1 on EBV-encoded latent gene expression. EBV gene expression was tested at 2 days post-infection by quantitative RT-PCR. We focused on the C/Wp activity because it expresses key viral transactivators including EBNA1, -2, -3s, and -LP to boost viral transforming gene expression. We detected C/Wp-driven transcripts in GFP Hi BALL-1 cells as expected. Conversely, C/Wp-driven transcripts were undetectable in GFP-dnE1 Hi and Lo BALL-1 cells, although these cells retained similar EBV DNA levels to GFP-expressing cells (Fig. 4 and Table 3). The Cp-driven transcript was under the limit of detection by RT-PCR, suggesting that the Wp is predominantly activated at the early phase of EBV infection consistent with previous findings.[7] Inhibition of viral gene transcription was not observed in the RNA polymerase III-driven transcript EBER1,[25] and cyclophilin A mRNA levels were similar between GFP- and GFP-dnE1-expressing cells (Fig. 4 and Table 3). This indicates that the effect of GFP-dnE1 on C/Wp activity is specific, and uncovers an active role of EBNA1 in supporting transactiva-

Table 2. The establishment efficiency of EBV latency

Cell	Emergence of G418-resistant cells†	
BJAB	100%	(6/6)
Daudi	100%	(10/10)
BALL-1		
Parental	56%	(5/9)
GFP Hi	67%	(2/3)
GFP-dnE1 Hi	0%	(0/6)
GFP-dnE1 Lo	0%	(0/6)

†Percentage of wells positive for G418-resistant cells over the number of tested wells from 96-well plates indicated in the bracket. Shown are the sum of two independent experiments. dnE1, dominant-negative EBNA1; EBV, Epstein–Barr virus; GFP, green fluorescent protein.

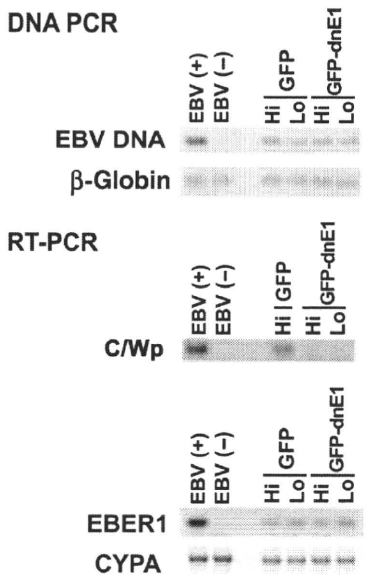

Fig. 4. PCR-based analysis of Epstein–Barr virus (EBV) gene expression. The effect of green fluorescent protein (GFP)-dominant-negative EBNA1 (dnE1) on the loss of EBV DNA (DNA PCR, upper panels) and transcription of the C/W promoter-driven transcript (C/Wp), EBER1, and cyclophilin A (CYPA; RT-PCR, lower panels) in BALL-1 cells at 2 days post-infection were examined. EBV-transformed B-lymphoblastoid cell line (B-LCL) and BJAB cells, denoted as EBV(+) and EBV(–), were used as positive and negative controls for viral DNA and RNA shown, respectively. β-Globin and CYPA were used as controls.

Table 3. Quantification of EBV transcripts in BALL-1 cells by real-time PCR at 2 days post-infection

BALL-1 cells		W1/2 exon (copies†)	EBER1 (copies‡)	CYPA (copies‡)
GFP	Hi	2.2	2.8×10^2	1.4×10^6
	Lo	NT§	0.8×10^2	1.0×10^6
GFP-dnE1	Hi	BLD¶	3.3×10^2	1.3×10^6
	Lo	BLD¶	1.2×10^2	1.5×10^6

†Copies per 13–14 ng total cellular RNA. ‡Copies per 200 ng total cellular RNA. §Not tested. ¶Below the limit of detection. CYPA, cyclophilin A; dnE1, dominant-negative EBNA1; EBV, Epstein–Barr virus; GFP, green fluorescent protein.

tion from C/Wp. Taken together, these results show that inhibition of EBNA1 functions strongly restricts EBV-encoded transforming gene expression and, although there is no detectable effect on the ROL of EBV DNA at the acute phase of viral infection, it blocks the establishment of EBV latency during the subacute phase.

Discussion

This is the first report describing the effect of EBNA1 inhibition from the onset of EBV infection in B cells. Unexpectedly, the dnE1 was unable to accelerate the ROL during the acute phase of EBV infection since dnE1 enhanced the loss of the oriP plasmid in the transient transfection assays.[10,11] In the subacute phase of EBV infection, the establishment of EBV latency was potently blocked by dnE1. In addition, we observed a strong repressive effect of dnE1 on the EBNA1-dependent enhancement of viral gene transcription from C/Wp during the early phase of EBV infection, similar to the transient transfection assays.[17] These data suggest that viral oncogene expression depends heavily on EBNA1 during the acute phase of viral infection, and that EBNA1 contributes little to EBV genome maintenance during this period. The results emphasize that an EBNA1 inhibitor should serve as an attenuator of viral oncogene expression since activation of C/Wp is the 'root' event of the positive feedback loop involved in the transactivation of viral transforming gene expression. In this regard, the EBNA1 inhibition approach could be superior to LMP-1 or EBNA2 inhibition.

If EBNA1 binding to oriP is essential for both the enhancement of viral gene transcription and for genome maintenance, what mechanism prevents dnE1 from affecting the ROL during the acute phase of EBV infection? It is likely that maintenance of the oriP replicon immediately after its introduction into cells is less efficient than in cells harboring an 'established' oriP replicon as an autonomously replicating plasmid. The ROL of an established oriP replicon is 2–4% per cell generation.[10,11] In contrast, our data from the EBV/B cell-based assay gave an average ROL of 26–38% during the week post-infection (acute phase of EBV infection). In agreement with our findings, it is reported that a transiently transduced oriP replicon is lost from cells at 26–37% per cell generation 1–2 weeks post-plasmid transduction.[12] These data indicate that maintenance of the oriP replicon is largely EBNA1-independent immediately after its introduction into cells, regardless of whether the route of introduction is by transfection or EBV infection. In other words, the establishment of EBV latency should be a rare epigenetic event. The data also suggest that the artificial minichromosome approach may be relevant in understanding EBV genome behavior.[12]

Our study suggests that gene therapy using GFP-dnE1 is an attractive approach, not only for therapeutics, but also for prophylactic interventions of EBV-associated malignancies. For example, in peripheral blood stem cell transplantation (PBSCT), GFP-dnE1 transduction into $CD34^+$ cells should protect the differentiated B cells from EBV infection, thus preventing the genesis of EBV-associated B cell lymphomas. We will attempt to prove this hypothesis using a small animal model in future studies.[26] Additionally, EBNA1 is a potential molecular target for developing a small molecular-weight EBV inhibitor as mentioned previously.[14,15] The advantages of EBNA1-inhibitor development are that the biological assay system is already established and the X-ray crystal structure of the DNA-bound EBNA1 DNA binding and dimerization domain is known, which means that computer-aided drug design technology can be immediately applied. Although EBV is associated with various malignancies, preventive and therapeutic measures against EBV infection have not been developed. We believe that an anti-EBV agent, such as an EBNA1 inhibitor, would have an enormous impact in the medical field due to the substantial number of patients with EBV-associated malignancies.

doi: 10.1111/j.1349-7006.2009.01474.x

Acknowledgments

We thank Drs Kenichi Imadome and Shigeyoshi Fujiwara for reagents. We also thank Dr Bill Sugden for critically reading the manuscript. This work was supported by the Japan Health Science Foundation, the Ministry of Health, Labor and Welfare of Japan, and the Ministry of Education, Culture, Sports, Science and Technology of Japan.

Disclosure Statement

The authors have no conflict of interest.

References

1 Thompson MP, Kurzrock R. Epstein–Barr virus and cancer. *Clin Cancer Res* 2004; **10**: 803–21.
2 Rickinson AB, Kieff E. Epstin–Barr virus. In: Knipe DM, Howley PM, eds. *Fields Virology*, 5th edn, vol. 2. Philadelphia: Lippincott Williams & Wilkins, 2007; 2655–700.
3 Klein E, Kis LL, Klein G. Epstein–Barr virus infection in humans: from harmless to life endangering virus-lymphocyte interactions. *Oncogene* 2007; **26**: 1297–305.
4 Snow AL, Martinez OM. Epstein–Barr virus: evasive maneuvers in the development of PTLD. *Am J Transplant* 2007; **7**: 271–7.
5 Besson C, Goubar A, Gabarre J *et al.* Changes in AIDS-related lymphoma since the era of highly active antiretroviral therapy. *Blood* 2001; **98**: 2339–44.
6 Carbone A, Cesarman E, Spina M, Gloghini A, Schulz TF. HIV-associated lymphomas and gamma-herpesviruses. *Blood* 2009; **113**: 1213–24.
7 Kieff E, Rickinson AB. Epstin–Barr virus and its replication. In: Knipe DM, Howley PM, eds. *Fields Virology*, 5th edn, vol. 2. Philadelphia: Lippincott Williams & Wilkins, 2007; 2603–54.
8 Lindner SE, Sugden B. The plasmid replicon of Epstein–Barr virus: mechanistic insights into efficient, licensed, extrachromosomal replication in human cells. *Plasmid* 2007; **58**: 1–12.
9 Wang J, Sugden B. Origins of bidirectional replication of Epstein–Barr virus: models for understanding mammalian origins of DNA synthesis. *J Cell Biochem* 2005; **94**: 247–56.
10 Kirchmaier AL, Sugden B. Plasmid maintenance of derivatives of oriP of Epstein–Barr virus. *J Virol* 1995; **69**: 1280–3.
11 Sugden B, Warren N. Plasmid origin of replication of Epstein–Barr virus, oriP, does not limit replication in cis. *Mol Biol Med* 1988; **5**: 85–94.
12 Leight ER, Sugden B. Establishment of an oriP replicon is dependent upon an infrequent, epigenetic event. *Mol Cell Biol* 2001; **21**: 4149–61.
13 Hurley EA, Thorley-Lawson DA. B cell activation and the establishment of Epstein–Barr virus latency. *J Exp Med* 1988; **168**: 2059–75.
14 Altmann M, Pich D, Ruiss R, Wang J, Sugden B, Hammerschmidt W. Transcriptional activation by EBV nuclear antigen 1 is essential for the expression of EBV's transforming genes. *Proc Natl Acad Sci U S A* 2006; **103**: 14188–93.
15 Kennedy G, Komano J, Sugden B. Epstein–Barr virus provides a survival factor to Burkitt's lymphomas. *Proc Natl Acad Sci U S A* 2003; **100**: 14269–74.
16 Nasimuzzaman M, Kuroda M, Dohno S *et al.* Eradication of Epstein–Barr virus episome and associated inhibition of infected tumor cell growth by adenovirus vector-mediated transduction of dominant-negative EBNA1. *Mol Ther* 2005; **11**: 578–90.
17 Kirchmaier AL, Sugden B. Dominant-negative inhibitors of EBNA-1 of Epstein–Barr virus. *J Virol* 1997; **71**: 1766–75.
18 Komano J, Miyauchi K, Matsuda Z, Yamamoto N. Inhibiting the Arp2/3 complex limits infection of both intracellular mature vaccinia virus and primate lentiviruses. *Mol Biol Cell* 2004; **15**: 5197–207.
19 Aiyar A, Sugden B. Fusions between Epstein–Barr viral nuclear antigen-1 of Epstein–Barr virus and the large T-antigen of simian virus 40 replicate their cognate origins. *J Biol Chem* 1998; **273**: 33073–81.
20 Middleton T, Sugden B. EBNA1 can link the enhancer element to the initiator element of the Epstein–Barr virus plasmid origin of DNA replication. *J Virol* 1992; **66**: 489–95.
21 Urano E, Kariya Y, Futahashi Y *et al.* Identification of the P-TEFb complex-interacting domain of Brd4 as an inhibitor of HIV-1 replication by functional cDNA library screening in MT-4 cells. *FEBS Lett* 2008; **582**: 4053–8.
22 Shimizu S, Urano E, Futahashi Y *et al.* Inhibiting lentiviral replication by HEXIM1, a cellular negative regulator of the CDK9/cyclin T complex. *AIDS* 2007; **21**: 575–82.
23 Kanda T, Yajima M, Ahsan N, Tanaka M, Takada K. Production of high-titer Epstein–Barr virus recombinants derived from Akata cells by using a bacterial artificial chromosome system. *J Virol* 2004; **78**: 7004–15.
24 Mackey D, Sugden B. The linking regions of EBNA1 are essential for its support of replication and transcription. *Mol Cell Biol* 1999; **19**: 3349–59.
25 Howe JG, Shu MD. Epstein–Barr virus small RNA (EBER) genes: unique transcription units that combine RNA polymerase II and III promoter elements. *Cell* 1989; **57**: 825–34.
26 Yajima M, Imadome K, Nakagawa A *et al.* A new humanized mouse model of Epstein–Barr virus infection that reproduces persistent infection, lymphoproliferative disorder, and cell-mediated and humoral immune responses. *J Infect Dis* 2008; **198**: 673–82.

Antiviral Research 90 (2011) 33–41

Contents lists available at ScienceDirect

Antiviral Research

journal homepage: www.elsevier.com/locate/antiviral

Within-host co-evolution of Gag P453L and protease D30N/N88D demonstrates virological advantage in a highly protease inhibitor-exposed HIV-1 case

Junko Shibata[a,b,1], Wataru Sugiura[b,c,d,*], Hirotaka Ode[e], Yasumasa Iwatani[b,c,d], Hironori Sato[e], Hsinyi Tsang[b], Masakazu Matsuda[d,f], Naoki Hasegawa[a], Fengrong Ren[a], Hiroshi Tanaka[a]

[a] School of Biomedical Sciences, Tokyo Medical and Dental University, Tokyo, Japan
[b] Clinical Research Center, National Hospital Organization, Nagoya Medical Center, Nagoya, Japan
[c] Nagoya University Graduate School of Medicine, Nagoya, Japan
[d] AIDS Research Center, National Institute of Infectious Diseases, Tokyo, Japan
[e] Pathogen Genomics Center, National Institute of Infectious Diseases, Tokyo, Japan
[f] Mitsubishi Chemical Medience Corporation, Tokyo, Japan

ARTICLE INFO

Article history:
Received 7 September 2010
Received in revised form
28 December 2010
Accepted 11 February 2011
Available online 19 February 2011

Keywords:
HIV
Protease
Gag
Drug resistance
Co-evolution

ABSTRACT

To better understand the mechanism of HIV group-specific antigen (Gag) and protease (PR) co-evolution in drug-resistance acquisition, we analyzed a drug-resistance case by both bioinformatics and virological methods. We especially considered the quality of sequence data and analytical accuracy by introducing single-genome sequencing (SGS) and Spidermonkey/Bayesian graphical models (BGM) analysis, respectively. We analyzed 129 HIV-1 Gag–PR linkage sequences obtained from 8 time points, and the resulting sequences were applied to the Spidermonkey co-evolution analysis program, which identified ten mutation pairs as significantly co-evolving. Among these, we focused on associations between Gag-P453L, the P5′ position of the p1/p6 cleavage-site mutation, and PR-D30N/N88D nelfinavir-resistant mutations, and attempted to clarify their virological significance *in vitro* by constructing recombinant clones. The results showed that $P453L^{Gag}$ has the potential to improve replication capacity and the Gag processing efficiency of viruses with $D30N^{PR}/N88D^{PR}$ but has little effect on nelfinavir susceptibility. Homology modeling analysis suggested that hydrogen bonds between the 30th PR residue and the $R452^{Gag}$ are disturbed by the $D30N^{PR}$ mutation, but the impaired interaction is compensated by $P453L^{Gag}$ generating new hydrophobic interactions. Furthermore, database analysis indicated that the $P453L^{Gag}/D30N^{PR}/N88D^{PR}$ association was not specific only to our clinical case, but was common among AIDS patients.

1. Introduction

Major mutations in the human immunodeficiency virus-1 (HIV-1) protease (PR)-coding region selected by protease inhibitors (PIs) are mainly located within the active sites of the PR, and these mutations significantly reduce PR activity and viral replication capacity, i.e., viral fitness, compared to that of wild-type strains (Mahalingam et al., 1999). However, PI-resistant viruses have the potential to undergo further selection and evolution to recover their impaired PR activity and viral fitness by acquiring additional mutations not only in the PR but also in its natural substrate, the Gag protein (Nijhuis et al., 1999). In particular, mutations in Gag cleavage sites can improve the replication capacity of PI-resistant viruses. Indeed, tight associations have been demonstrated between PI-resistant mutations and Gag cleavage-site mutations, such as $S373Q^{Gag}$ (Malet et al., 2007) and $I376V^{Gag}$ (Ho et al., 2008) at p2/NC, $A431V^{Gag}$ (Bally et al., 2000; Doyon et al., 1996; Gallego et al., 2003; Koch et al., 2001; Maguire et al., 2002; Malet et al., 2007; Verheyen et al., 2006; Zhang et al., 1997) at NC/p1, $L449F^{Gag}$ (Doyon et al., 1996), and $P453L^{Gag}$ (Bally et al., 2000; Maguire et al., 2002; Verheyen et al., 2006) at p1/p6. Gag mutations at non-cleavage sites have also been reported to improve the fitness of PI-resistant viruses (Myint et al., 2004). Thus, the selection and evolution of Gag and PR are accepted to significantly interfere with each other. This phenomenon is known as "Gag–PR co-evolution."

However, previous reports of Gag–PR co-evolution appear to have two technical limitations related to data quality and analytical method. First, the standard population-based genotyping method commonly used for determining HIV-1 variants has limited accuracy for technological reasons. To sequence the viral genome,

* Corresponding author at: Clinical Research Center, National Hospital Organization, Nagoya Medical Center, 4-1-1, San-no-maru, Naka-ku, Nagoya, Aichi 4600001, Japan. Tel.: +81 52 951 1111; fax: +81 52 963 3970.
E-mail address: wsugiura@nih.go.jp (W. Sugiura).
[1] Current address: Inserm U941, IUH, Université Paris Diderot, Hôpital Saint Louis, 75475 Paris Cedex 10, France.

0166-3542/$ – see front matter © 2011 Elsevier B.V. All rights reserved.
doi:10.1016/j.antiviral.2011.02.004

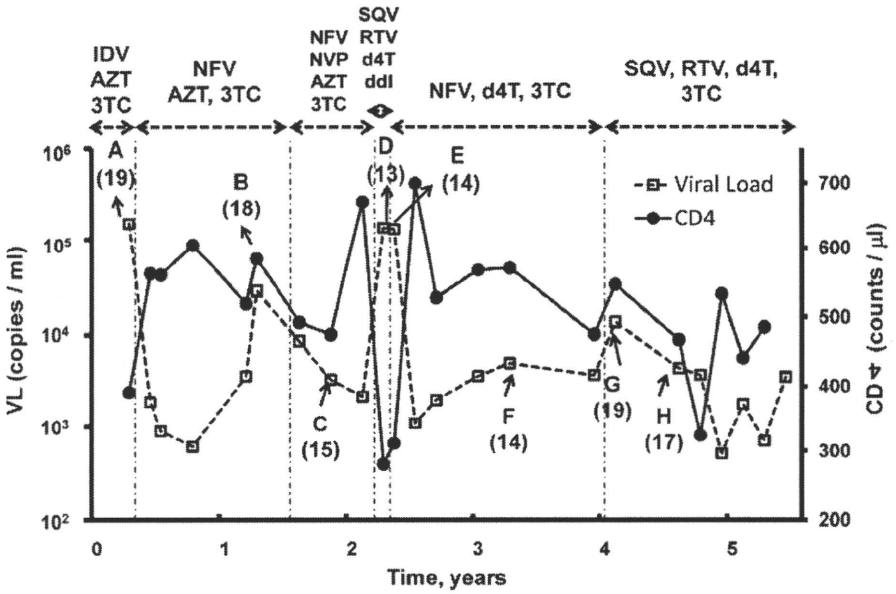

Fig. 1. Clinical course of patient-treatment protocols. Open squares and solid circles indicate plasma viral load and CD4+ cell count, respectively. Each treatment regimen is indicated in the upper part of the graph by horizontal dashed lines between arrows. Sample collection points are labelled A to H, and numbers of sequences analyzed at each point are shown in parentheses. AZT, zidovudine; d4T, stavudine; ddI, didanosine; 3TC, lamivudine; NVP, nevirapine; NFV, nelfinavir; RTV, ritonavir; SQV, saquinavir; IDV, indinavir.

viral RNA from patient plasma must be reverse-transcribed to cDNA, and the target regions are then amplified by PCR. Since viral cDNA includes multiple viral populations, using such samples as a template for the PCR step followed by sequencing results in amplification of predominantly the major variants (Gunthard et al., 1998; Hance et al., 2001), which may not represent the diversity of the original population. Furthermore, there is always a risk of artificial recombination of viral cDNAs, which are estimated to occur at rates of 4–70% during the PCR step (Meyerhans et al., 1990) and may disturb the linkage of mutation sites. Thus, this artificial linkage information may significantly affect the results of co-evolution analyses. To circumvent this technical problem, we employed the single-genome sequencing (SGS) technique based on limiting-dilution assays (Palmer et al., 2005). With SGS, artificial recombination can be avoided during PCR because cDNA samples are diluted after the reverse transcriptase reaction to a single cDNA molecule, which is used as the PCR template. Therefore, the viral sequence information obtained by SGS is not only more sensitive for analyzing HIV population diversity and mutation linkages than that obtained by standard genotype analysis, but also more precise for identifying co-evolving sites.

Second, many analytical methods have been developed for detecting co-evolving sites in molecular sequences. However, early methods did not accommodate the evolutionary history among sequences, and risked generating false-positive predictions (Altschuh et al., 1987; Gutell et al., 1992; Martin et al., 2005; Neher, 1994; Pollock and Taylor, 1997; Tillier and Lui, 2003). In recent years, the accuracy of estimating co-evolving sites has greatly improved due to several computational algorithms that incorporate the phylogenetic relationships among molecular data (Bhattacharya et al., 2007; Dutheil et al., 2005; Poon et al., 2008; Tuff and Darlu, 2000; Wollenberg and Atchley, 2000; Yeang and Haussler, 2007). In particular, Spidermonkey analysis (Poon et al., 2007a,b, 2008) not only considered the phylogenetic relationships but also implemented two empirical HIV-1 subtype B amino acid-substitution models for describing between- and within-host HIV evolution (Nickle et al., 2007).

In this study, we clarified the impact of Gag and PR co-evolution in the acquisition of drug resistance by inferring co-evolving sites between Gag and PR in a dataset of HIV-1 Gag–PR linkage sequences from a single patient who had undergone highly active antiretroviral therapy (HAART) for a long period. We used the SGS method for sequencing viral samples to avoid artificial recombination, and applied Spidermonkey analysis to our data by using its option for the within-host HIV substitution model. Virological significance of the estimated co-evolving sites was analyzed *in vitro* by constructing recombinant viruses on a pNL4-3 backbone. The replication kinetics, susceptibility to anti-HIV drugs, and the Gag processing efficiency were evaluated for each clone. We also conducted homology modeling analysis to examine Gag–PR interactions and database analysis to confirm the universality of the co-evolving sites.

2. Materials and methods

2.1. Sample collection and gag-PR-coding region sequencing by single-genome sequencing

From all HIV/AIDS patients monitored from April 1998 to August 2002 at the National Institute of Infectious Diseases in Japan, we selected a virological failure case with a history of multiple antiretroviral treatments. Of all cases, this one had been followed for the longest period and had enough detailed clinical information to perform our analysis. For the selected case, we collected plasma samples and clinical information, such as treatment regimens, changes in viral load, and CD4 counts (Fig. 1).

The single-genome sequencing (SGS) method was used as described (Palmer et al., 2005). Briefly, HIV-1 RNA was extracted from plasma samples (containing a minimum of 1000 copies of HIV-1 RNA) by guanidinium isothiocyanate treatment. cDNA was synthesized using Superscript II RT kit (Invitrogen, Carlsbad, CA) and a random hexamer. cDNA was serially diluted and amplified by PCR and nested PCR using Platinum Taq DNA Polymerase High Fidelity (Invitrogen). The endpoint of reverse-transcribed cDNA was determined as a single clone by the Poisson distribution, with cDNA dilutions yielding PCR products in 3 out of 10 reactions. The following primer sets were used in the first and nested PCR amplifications: first PCR-WGPF1 (5′-CTCTCTCGACGCAGGACTCG-

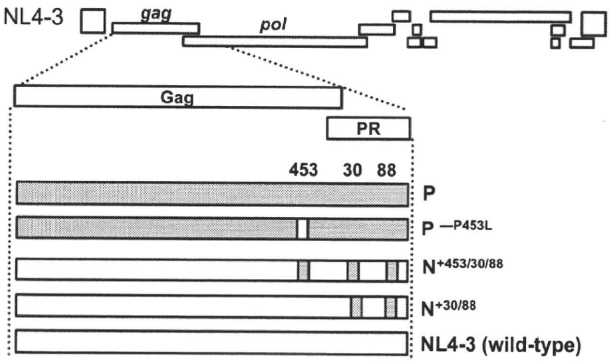

Fig. 2. Construction of recombinant viruses. Four different types of recombinant viruses were constructed according to their mutation patterns: (1) P, NL4-3 backbone with patient-derived Gag and protease (PR); (2) P^{-453}, NL4-3 backbone with patient-derived Gag and PR but $P453L^{Gag}$ was converted to wild-type; (3) $N^{+453/30/88}$, NL4-3 backbone including the substitutions $P453L^{Gag}$, $D30N^{PR}$, and $N88D^{PR}$; (4) $N^{+30/88}$, NL4-3 backbone including the substitutions $D30N^{PR}$and $N88D^{PR}$.

3′) and 3500- (5′-CTATTAAGTATTTTGATGGGTCATAA-3′), nested PCR-WGPF2 (5′-TTGCTGAAGCGCGCACGGCAAGA-3′) and 3410-(5′-CAGTTAGTGGTATTACTTCTGTTAGTGCTT-3′). These primer sets amplified a 2.7 kbps fragment containing *gag*, the PR-coding region of *pol*, and the first 900 nucleotides of the reverse transcriptase-coding region of *pol*. Positive PCR products were determined by agarose gel electrophoresis and sequenced using ABI Prism BigDye Terminator version 3.1 dideoxyterminator cycle sequencing (Applied Biosystems, Carlsbad, CA). Sequences, including the entire *gag* gene (1500 bp) and PR-coding region (297 bp), were aligned on the HXB2 reference using Sequence Navigator software (Applied Biosystems). Sequences containing mixtures at any position were excluded from analysis. PI-resistant mutations and other PR mutations in our data set were determined using the Calibrated Population Resistance tool Version 4.3 beta (http://cpr.stanford.edu/cpr/).

2.2. Detecting co-evolution using Spidermonkey analysis

Co-evolving sites between Gag and PR were inferred using Spidermonkey analysis (Poon et al., 2007a,b, 2008) to analyze all sequences (data type = protein), including the entire Gag (500 amino acids) and PR (99 amino acids) sequences. A phylogenetic tree was first reconstructed using the neighbor-joining method (Saitou and Nei, 1987). To infer co-evolving sites, we selected the within-host HIV protein-substitution model (frequencies: model-defined), based on the maximum likelihood method (Nickle et al., 2007). Amino acid sequences at MA/CA, CA/p2, p2/NC, NC/p1, and p1/p6 Gag cleavage-sites (residues P5 to P5′) and the complete PR sequence were selected for BGM analysis. We used the default options for calculations and inferred co-evolving sites if the estimated posterior probability for a pair of positions exceeded the cutoff value of 0.5.

2.3. Construction of recombinant HIV with a patient-derived gag-PR-coding region

To confirm the contributions of $P453L^{Gag}$ in the context of patient-derived *gag*-PR-coding region, three types of recombinant viruses were constructed (Fig. 2). Recombinant viruses were constructed using the pNL4-3 molecular clone of HIV-1 (GenBank accession No. AF324493). A patient-derived *gag*-PR-coding region containing $P453L^{Gag}$, $D30N^{PR}$, and $N88D^{PR}$ was chosen from sampling point F. The recombinants were (1) P, NL4-3 backbone with patient-derived *gag*-PR-coding region; (2) P^{-P453L}, NL4-3 backbone with patient-derived *gag*-PR-coding region but $P453L^{Gag}$ was converted to wild-type.

Details of the recombinant virus construction were as follows. The patient-derived 1.9 kbp *gag*-PR-coding region was subcloned into pCR4-TOPO (Invitrogen) (designated $pCR4\text{-}TOPO^{Patient}$). Using $pCR4\text{-}TOPO^{Patient}$ as a template, $P453L^{Gag}$ was substituted with wild-type P453. Each substitution was introduced using the following primer sets: For the Gag-P453 substitution, forward: 5′-TTCAGAACAGACCAGAGCCATCAGCT-3′, reverse: 5′-AGCTGATGGCTCTGGTCTGTTCTGAA-3′. Subsequently, the substituted *gag*-PR-coding region was amplified using the following primers: WGPF2: 5′-TTGCTGAAGCGCGCACGGCAAGA-3′ and DRPRO6: 5′-ACTTTTGGGCCATCCATTCCTGGCTTT-3′. The NL4-3-derived RT-coding region was amplified using the following primers: RT-63F: 5′-TAAACAATGGCCATTGACAGAAG-3′ and RT-898R: 5′-CTGCTTCTTCTGTTAGTGGTACTAC-3′. Primers DRPRO6 and RT-63F are phosphorylated at their 5′ ends. Both resulting fragments were ligated and digested with BssHII and SbfI, and cloned back into pNL4-3. All pNL4-3-based recombinant DNAs (3.75 μg) were transfected into 2×10^5 HeLa cells using Fugene6 (Roche, Indianapolis, IN), and culture supernatants were harvested at 72 h after transfection, filtered through a 0.45 μm membrane, assayed for reverse transcriptase (RT) activity (Willey et al., 1988), and kept as virus stocks at −80 °C until use. Each virus stock (5×10^6 ^{32}P cpm of RT activity) was used for replication kinetics analyses.

2.4. Construction of pNL43 with $P453L^{Gag}$, $D30N^{PR}$, and $N88D^{PR}$ by site-directed mutagenesis

In addition to constructing patient-derived *gag*-PR-coding region recombinant viruses, we evaluated the effect of $P453L^{Gag}$, $D30N^{PR}$, and $N88D^{PR}$ interference by constructing three types of pNL4-3-based recombinant viruses (Fig. 2). These were (1) $N^{+453/30/88}$, NL4-3 including $P453L^{Gag}/D30N^{PR}/N88D^{PR}$; and (2) $N^{+30/88}$, NL4-3 including $D30N^{PR}/N88D^{PR}$. These recombinant viruses were constructed as follows. pCR4-TOPO (Invitrogen) including the ApaI-SbfI fragment of pNL4-3, which contained the complete p1/p6 of *gag* and PR-coding region, was constructed as a template for further mutagenesis. This construct was designated as $pCR4\text{-}TOPO/NL^{ApaI\text{-}SbfI}$. Using $pCR4\text{-}TOPO/NL^{ApaI\text{-}SbfI}$ as a template, we introduced three mutations ($P453L^{Gag}$, $D30N^{PR}$, and $N88D^{PR}$) by site-directed mutagenesis. The following primer sets were used to introduce each mutation: For $P453L^{Gag}$, forward: 5′-TTCAGAGCAGACTAGAGCCAACAGCC-3′ and reverse: 5′-GGCTGTTGGCTCTAGTCTGCTCTGAA-3′. For $D30N^{PR}$, forward: 5′-CAGGAGCAGATAATACAGTATTAGAAG-3′ and reverse: 5′-CTTCTAATACTGTATTATCTGCTCCTG-3′. For $N88D^{PR}$, forward: 5′-CATAATTGGAAGAGATCTGTTGACTC-3′ and reverse: 5′-GAGTCAACAGATCTCTTCCAATTATG-3′. After each mutagenesis reaction, the entire sequences were verified and cloned back into pNL4-3 using ApaI and SbfI restriction enzymes. All pNL4-3-based recombinant DNAs (3.75 μg) were transfected into 2×10^5 HeLa cells using Fugene6 (Roche), and culture supernatants were harvested at 72 h after transfection, filtered through a 0.45 μm membrane, assayed for RT activity (Willey et al., 1988), and kept as virus stocks at −80 °C until use. Each virus stock (4×10^5 ^{32}P cpm of RT activity) was used for replication kinetics analysis.

2.5. Replication kinetics of recombinant viruses

Replication kinetics of recombinant viruses was evaluated as described (Matsuoka-Aizawa et al., 2003). Briefly, 5×10^4 MT-2 cells were infected with each virus stock in the absence or presence of 0.1 μM nelfinavir at 37 °C for 16 h. Cells were then washed once and resuspended in 0.5 ml culture medium with the same concen-

tration of nelfinavir, and cultures were maintained for 12–22 days, changing half of the medium every 2 or 3 days. The titer of each virus was evaluated by both RT activity and p24 amount; as both measures demonstrated good correlation, p24 amount was used to adjust the virus inoculum. Culture supernatants were collected, and residual supernatants were kept at −80 °C until use. Replication kinetics was independently analyzed two times.

2.6. Evaluation of nelfinavir susceptibilities of recombinant viruses

Recombinant viruses were evaluated for nelfinavir susceptibility using an in-house drug susceptibility assay with the MaRBLE cell line (MaRBLE assay) as described (Chiba-Mizutani et al., 2007). Briefly, 1×10^5 MaRBLE cells were infected with 100 $CCID_{50}$ of each recombinant virus, and virus replication was monitored in serial dilutions of nelfinavir from 1.28×10^{-13} to 1.0×10^{-6} M for 7 days in triplicate. At day 7, cells were harvested and lysed in luciferase assay reagent. Firefly (FF) and renilla luciferase (RF) activities produced by the cells were quantified using a Dual-luciferase Reporter Assay System (Promega, Madison, WI). The relative virus replication rate (% replication) at each drug concentration was calculated by the following formula: % replication = (observed FF luciferase activity with drug − background [mock] FF luciferase activity)/(observed FF luciferase activity without drug − background [mock] FF luciferase activity) × 100. IC_{50} values were calculated with 95% confidence intervals using GraphPad Prism software and nonlinear regression analysis fitted with a sigmoidal dose–response curve with variable slope.

2.7. Analysis of Gag processing patterns in recombinant viruses

The Gag processing patterns of recombinant viruses were analyzed as described (Sugiura et al., 2002) with minor modifications. In brief, NL4-3-based recombinant DNAs (18 μg) was transfected into 5×10^6 HeLa cells using Fugene6 (Roche). The culture supernatants were harvested at 48 h after transfection with a culture medium change at 12 h post transfection to the absence or presence of 0.1 μM nelfinavir. For pelleting virus through a sucrose cushion, 25 ml of cell culture medium was layered onto 10 ml of 20% sucrose (wt/vol, in PBS) before centrifugation at 30,000 rpm in a swing rotor for 1.5 h. The medium and cushion were discarded, and the virus pellet was dissolved in 200 μl Laemmli sample buffer (Bio-Rad, Hercules, CA). Viral supernatants were normalized using PETRO-TEK HIV-1 p24 Antigen ELISA (ZeptoMetrix Corporation, Buffalo, NY) and subjected to sodium dodecyl sulfate polyacrylamide gel electrophoresis (SDS–PAGE). Proteins in the gels were passively transferred to PVDF membranes (Bio-Rad). The membranes were incubated with a chicken anti-p6 polyclonal antibody (Sigma–Aldrich Corporation, St. Louis, MO) and a murine anti-p24 monoclonal antibody (ZeptoMetrix Corporation) for 2 h, followed by incubation with secondary antibody, a chicken HRP-conjugated, IgG antibody (Bethyl Laboratories Inc., Montgomery, TX), a mouse HRP-conjugated, IgG antibody (Thermo Fisher Scientific, Yokohama, JP), respectively. Finally, proteins were visualized using SuperSignal West Dura Extended Duration Substrate (Thermo Fisher Scientific).

2.8. Molecular modeling of Gag p1/p6 peptide–PR complexes

We constructed three-dimensional models of PR in complex with peptide representing Gag-p1/p6 substrate by a homology modeling method (Baker and Sali, 2001; Marti-Renom et al., 2000; Shirakawa et al., 2008) using Molecular Operating Environment (MOE) ver. 2008.10 (http://www.chemcomp.com/, Chemical Computing Group Inc., Montreal, Quebec, Canada). For the modeling template, we used an X-ray crystal structure of inactive D25N PR in complex with the p1/p6 substrate at 2 Å resolution (PDB code: 1KJF) (Prabu-Jeyabalan et al., 2002), as it had the highest similarity (94.2% identity) to the HIV-1 NL4-3 strain among HIV-1 protease-p1/p6 peptide structures in the protein data bank, even though this is an inactive model. Furthermore, the active-site $D25N^{PR}$ mutation has been reported to hardly influence the structure of the protease in complex with ligands (Sayer et al., 2008). In the models, nine-amino-acid-length peptides corresponding to the Gag p1/p6 of the NL4-3, $N^{+30/88}$, and $N^{+453/30/88}$ strains were bound to the catalytic sites of PRs of the same strains. We considered effects of a water molecule (HOH11) that mediates important hydrogen bonds between the Gag p1/p6 peptide and the PR. AMBER ff99 force field (Wang et al., 2000) and generalized Born/volume integral (GB/VI) implicit solvent model (Labute, 2008) were applied for intra- and inter-molecular energy calculations.

2.9. Database analysis

To confirm the universality of $P453L^{Gag}/D30N^{PR}/N88D^{PR}$, we obtained 3249 sequences of HIV-1 subtype B *gag*-PR-coding region (positions 2146–2516) from the Los Alamos National Laboratory HIV sequence database (http://www.hiv.lanl.gov/). For the dataset, we applied Fisher's exact test and investigated associations between the D30N/N88D mutations in PR and the P453L mutation in Gag and between the 30/88 mutations in PR and the P453L mutation in Gag, respectively. Fisher's exact test was implemented using the R 2.6.1 statistical package.

3. Results

3.1. The majority of patient-derived Gag cleavage-site mutations are in p2/NC and p1/p6

Twenty-three plasma samples were serially collected from a patient who had received HAART for 52 months. The patient's clinical history, changes in viral load, and CD4 counts are depicted in Fig. 1. At 8 sampling points (A–H), 129 *gag*-PR-coding region sequences were obtained, with p2/NC and p1/p6 Gag cleavage-site mutations observed at each point in more than 60% of clones (Table 1). PI-resistant mutations and other PR mutations are also summarized in Table 1. None of the clones had CA/p2 cleavage-site mutations, and only a few clones had MA/CA or NC/p1 cleavage-site mutations. The $Y132F^{Gag}$ mutation in MA/CA was found in 1.6% of the clones, and $E428D^{Gag}$ and $R429K^{Gag}$ within NC/p1 had prevalences of 1.6% and 5.4%, respectively. On the other hand, cleavage-site mutations were frequently observed within p2/NC and p1/p6. In the p2/NC site, we observed 11 mutations: $S373Q^{Gag}$ (83.7%), $S373P^{Gag}$ (15.5%), $A374G^{Gag}$ (79.8%), $A374V^{Gag}$ (16.3%), $A374S^{Gag}$ (2.3%), $A374R^{Gag}$ (0.8%), $T375N^{Gag}$ (100%), $I376V^{Gag}$ (3.9%), $M378L^{Gag}$ (0.8%), $G381S^{Gag}$ (0.8%), and $N382Y^{Gag}$ (0.8%). In the p1/p6 site, we observed three mutations: $L449F^{Gag}$ (0.8%), $S451N^{Gag}$ (100%), and $P453L^{Gag}$ (65.1%).

3.2. Ten Gag–protease co-evolving sites are inferred by Spidermonkey analysis

Among the 129 *gag*-PR-coding region sequences analyzed by Spidermonkey analysis (Poon et al., 2007a,b, 2008), ten co-evolving sites were inferred. These sites were identified using the default cutoff posterior probability (pp) value of 0.5. The ten co-evolving pairs identified with pp > 0.5 are shown in Table 2. Four pairs, $R429K^{Gag}/M36V^{PR}$ (pp = 0.87), $S373Q^{Gag}/T12A^{PR}$ (pp = 0.83), $P453L^{Gag}/D30N^{PR}$ (pp = 0.63), and $P453L^{Gag}/N88D^{PR}$ (pp = 0.61), represented Gag/PR inter-molecular co-evolution;

Table 1
Gag cleavage-site mutations and PR mutations from a HAART-treated case.

Sampling point	Gag cleavage-site mutation (%)[a]		PR mutation (%)[a]	
	p2/NC	p1/p6	PI-resistant mutations	Other PR mutations
A to H (n = 129)	T375N	S451N	–	I62V, L63P,A71T, I93L
A (n = 19)	S373Q(100), A374G (89),	–	–	M36I(95), I72V(11), V77I(100)
B (n = 18)	S373Q(100), A374G (94)	P453L(100)	D30N(100), M46I(6), N88D(100)	E35D(94), M36I(100), V77I(100),
C (n = 15)	S373Q(100), A374G(100)	P453L(100)	D30N(100), N88D(100)	L10F(80), E35D(100), M36I(100), K45R(27), I72T(7), V77I (100),
D (n = 13)	S373P (85), A374V (85)	P453L (8)	D30N (8), N88D (8)	L10F(8), V11I (8), T12A(8), K20R(8), E35D(8), M36I(100), H69Y(8), V77I(8)
E (n = 14)	S373P (64), A374V(71)	–	–	T12A(7), M36I(100), K55N (7), V77I(7)
F (n = 14)	S373Q(100), A374G(100)	P453L(100)	D30N(100), N88D(100)	L10F(100), I13V(79), E34G(7), E35D(100), M36I (100), N37T (86), K45R (14), Q58E (86), I72T (7), V77I (100)
G (n = 19)	S373Q(100), A374G(100)	P453L(100)	D30N(100), N88D(100)	L10F(100), I13V (68), E35D(100), M36I(68), M36V(32), N37T(100), Q58E(100), V77I(100)
H (n = 17)	S373Q(100), A374G(100)	P453L(100)	D30N(100), I54V(76), N88D(100), L90M (47)	L10F(100), I13V (94), K20R (76), E35D (100), M36I (94), M36V (6), N37T (100), Q58E (100), I72T (53), V77I (100), G78R (6)

Gag mutations refer to HXB2 and PI-resistant mutations and other PR mutations were determined using the Calibrated Population Resistance tool Version 4.3 beta.
[a] Numbers in parentheses are the percentages of mutations at each sampling point.

one pair, $S373Q^{Gag}/A374G^{Gag}$, represented Gag/Gag intra-molecular co-evolution; and the other five pairs, $N37T^{PR}/Q58E^{PR}$ (pp = 0.94), $E35D^{PR}/M46I^{PR}$ (pp = 0.89), $K20R^{PR}/I54V^{PR}$ (pp = 0.88), $V11I^{PR}/K20R^{PR}$ (pp = 0.86), and $D30N^{PR}/N88D^{PR}$ (pp = 0.62), represented PR/PR intra-molecular co-evolution.

We focused on three pairs, $P453L^{Gag}/N88D^{PR}$, $P453L^{Gag}/D30N^{PR}$, and $D30N^{PR}/N88D^{PR}$, because $D30N^{PR}$ and $N88D^{PR}$ are well-known major and minor nelfinavir-resistant mutations, respectively (Johnson et al., 2008), and $P453L^{Gag}$ is the P5′ position of the p1/p6 cleavage-site mutation. Although $D30N^{PR}$ has been associated with $N88D^{PR}$ (Rhee et al., 2007; Wu et al., 2003), the interactions among $P453L^{Gag}$, $D30N^{PR}$, and $N88D^{PR}$ have not been investigated. Since $P453L^{Gag}/D30N^{PR}/N88D^{PR}$ was frequently observed in the presence of nelfinavir (Fig. 1 and Table 1), we conducted *in vitro* experiments to confirm whether the co-existence of $P453L^{Gag}/D30N^{PR}/N88D^{PR}$ has a virological advantage in the presence of nelfinavir.

3.3. $P453L^{Gag}$ improves the replication capacity of viruses with $D30N^{PR}/N88D^{PR}$ in both patient- and NL4-3-derived genetic backgrounds

To evaluate the virological impact of $P453L^{Gag}$ in the patient-derived genetic background, we constructed two types of patient-derived *gag*-PR-coding region viruses, P and P^{-P453L} (Fig. 2). These two recombinant viruses and the wild-type virus (NL4-3) were cultured independently in the absence or presence of nelfinavir, and their replication kinetics was monitored by measuring RT activity in culture supernatants. Assays for replication kinetics were independently performed twice, confirming identical orders of replication kinetics.

Table 2
Positions of coevolving pairs inferred by Spidermonkey analysis.

Position	Position	Expected posterior probability	Total number of sequences
429^{Gag}	36^{PR}	0.866	7
373^{Gag}	12^{PR}	0.825	2
453^{Gag}	30^{PR}	0.632	84
453^{Gag}	88^{PR}	0.607	84
373^{Gag}	374^{Gag}	0.895	22
37^{PR}	58^{PR}	0.938	48
35^{PR}	46^{PR}	0.887	1
20^{PR}	54^{PR}	0.877	13
11^{PR}	20^{PR}	0.858	1
30^{PR}	88^{PR}	0.618	84

Significant coevolving sites (pp value > 0.5) are shown.

In the absence of nelfinavir (Fig. 3A), the RT activities of the NL4-3 and P viruses peaked at 6 days after infection, and the RT activity of NL4-3 was higher than that of the P virus, whereas viral replication was delayed in the P^{-P453L} virus (i.e., P virus without $P453L^{Gag}$), and its RT activity peaked at 10 days after infection. The order of replication kinetics in the absence of nelfinavir was wild-type (NL4-3) > P > P^{-P453L}. On the other hand, in the presence of nelfinavir (Fig. 3B), replication of the wild-type virus was completely suppressed, and replication of P virus was the most active, demonstrating peak RT activity at 6 days after infection. The P^{-P453L} virus showed lower replication capacity than the P virus. Thus, the order of replication kinetics in the presence of nelfinavir was P > P^{-P453L} > wild-type (NL4-3).

To assess whether the complex $P453L^{Gag}/D30N^{PR}/N88D^{PR}$ conferred an advantage not only in the patient-derived genetic background but also in the HIV-1 molecular clone (NL4-3)-derived genetic background, we constructed two types of NL4-3-based *gag*-PR-coding region recombinant viruses, $N^{+453/30/88}$ and $N^{+30/88}$ (Fig. 2). The results of independent culture studies are shown in Fig. 3C and D. In the absence of nelfinavir, the RT activities of NL4-3, NL4-3 with $P453L^{Gag}/D30N^{PR}/N88D^{PR}$ ($N^{+453/30/88}$) and NL4-3 with $D30N^{PR}/N88D^{PR}$ ($N^{+30/88}$) viruses peaked at 11 days, 14 days, and 16 days after infection, respectively, and the order of replication kinetics was NL4-3 > $N^{+453/30/88}$ > $N^{+30/88}$. On the other hand, in the presence of nelfinavir, the $N^{+453/30/88}$ virus grew the most actively with its peak RT activity at 14 days after infection. The $N^{+30/88}$ virus was the second most actively replicating, and the wild-type did not replicate. Thus, the order of replication kinetics in the presence of nelfinavir was $N^{+453/30/88}$ > $N^{+30/88}$ > NL4-3.

In both studies, not only in the patient-derived genetic background but also in the NL4-3-derived genetic background, the virus with $D30N^{PR}/N88D^{PR}$ showed lower replication capacity than the virus with $P453L^{Gag}/D30N^{PR}/N88D^{PR}$, suggesting that $P453L^{Gag}$ significantly contributes to the fitness recovery of virus with $D30N^{PR}/N88D^{PR}$.

3.4. $P453L^{Gag}$ does not influence susceptibility to nelfinavir

To clarify whether $P453L^{Gag}$ affects nelfinavir susceptibility, the IC_{50}s of nelfinavir for NL4-3-based *gag*-PR-coding region recombinants were determined using MaRBLE cells. Both $N^{+453/30/88}$ and $N^{+30/88}$ recombinants showed 14.4 and 15.8-fold greater resistance to nelfinavir than wild-type virus, respectively (Table 3). However, the difference in IC_{50} between the two recombinants was

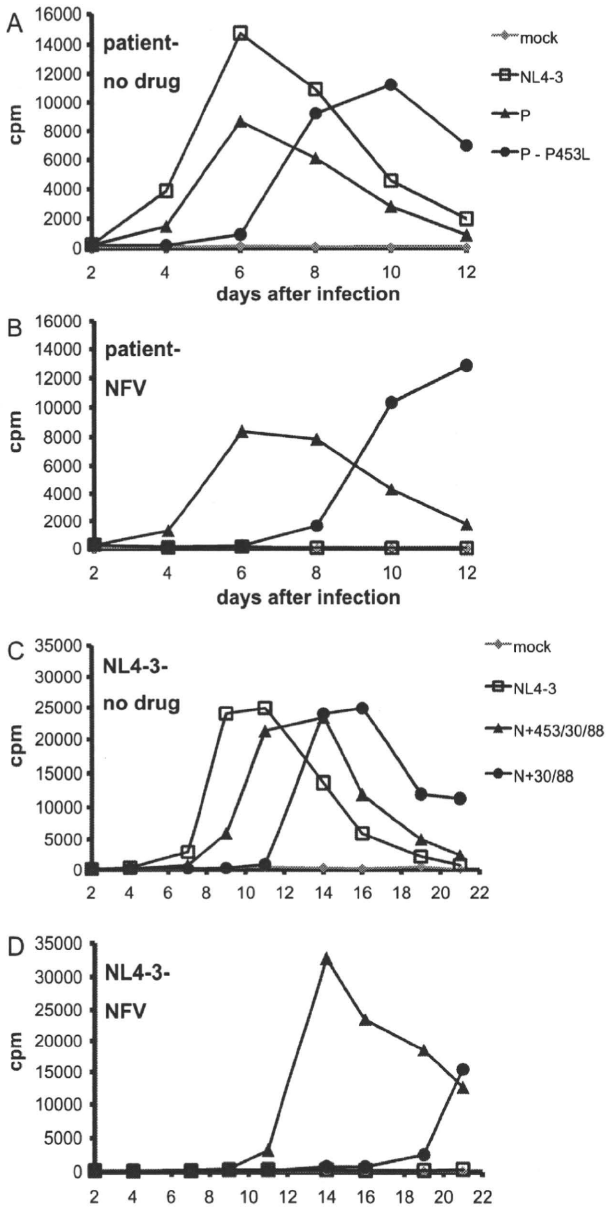

Fig. 3. Replication kinetics of recombinants. MT-2 cells were infected with patient-derived *gag*-PR-coding region, (A) in the absence of, and (B) in the presence of 0.1 μM nelfinavir. Open squares, solid triangles, and solid circles indicate wild-type NL4-3, NL4-3 with patient *gag*-PR-coding region insert, and NL4-3 with patient insert without P453L substitution, respectively. MT-2 cells were also infected with NL4-3-based recombinant, (C) in the absence of, and (D) in the presence of 0.1 μM nelfinavir. Open squares, solid triangles, and solid circles indicate wild type NL4-3; NL4-3 with P453L, D30N, and N88D; and NL4-3 with D30N and N88D, respectively. Diamonds indicate mock-infected controls. Assays were independently performed twice, and one representative set of results is shown.

not significant, suggesting that P453L^{Gag} had no effect on nelfinavir susceptibility.

3.5. *P453L^{Gag} improves Gag p1/p6 processing in virus with D30N^{PR}/N88D^{PR}*

To gain further insights into the virological effects of P453L^{Gag}, we examined Gag processing patterns in the absence and presence of 0.1 μM nelfinavir by Western blot analysis with an anti-p6 polyclonal antibody and an anti-p24 monoclonal antibody. The amount of sample loaded in each lane was normalized by p24 antigen content (600 ng for each lane as determined by ELISA) (Fig. 4A). In the absence of nelfinavir, the partially cleaved Gag intermediate p15 (including NC, p1, and p6) of NL4-3 was efficiently cleaved to the p6 peptide (Fig. 4B, lane 3). In contrast, the processing of NL4-3 was less efficient in the presence of nelfinavir, as indicated by the accumulation of p15 (Fig. 4B, lane 4). N$^{+30/88}$ showed defects in cleavage at the p1/p6 site, as demonstrated by the accumulation of p15 and p7 (p1/p6) (Fig. 4B, lanes 5 and 6). On the other hand, lesser p15 and p7 accumulated in N$^{+453/30/88}$ than in N$^{+30/88}$ (Fig. 4, lanes 7 and 8). Interestingly, a 8–9 kDa band, which is neither p6 nor p7, was observed in N$^{+30/88}$ (Fig. 4B, lanes 5 and 6).

Table 3
Nelfinavir susceptibilities of recombinant viruses.

HIV-1	IC_{50} (nM)	95% confidence interval	Fold-resistance
NL4-3	1.3	0.8–2.4	1.0
NL$^{+453/30/88}$	18.7	9.2–37.8	14.4
N$^{+30/88}$	20.6	12.6–33.6	15.8

3.6. *Impaired Gag–PR affinity in the N$^{+30/88}$ strain is recovered by new L453^{Gag} interactions with M46$'^{PR}$ and F53$'^{PR}$*

To elucidate the structural impact of the mutations described above on interactions between Gag-p1/p6 substrate and PR, we generated three-dimensional models of the PR in complex with peptide representing Gag-p1/p6 substrate by homology modeling (Baker and Sali, 2001; Marti-Renom et al., 2000; Shirakawa et al., 2008) using Gag and PR sequences of the NL4-3, N$^{+30/88}$, and N$^{+453/30/88}$ strains. Comparison of the thermodynamically optimized models showed obvious differences in interactions between side chains of PR and p1/p6 (Fig. 5). First, D30N^{PR} mutation resulted in fewer hydrophilic interactions between side chains of the 30th PR and 452nd p1/p6 residues; NL4-3 had two hydrogen bonds between the side chains of D30^{PR} and R452^{Gag} (Fig. 5A), while N$^{+30/88}$ and N$^{+453/30/88}$ had only a single hydrogen bond between the side chains of N30^{PR} and R452^{Gag} (Fig. 5B and C). Second, the P453L^{Gag} mutation in the p1/p6 substrate of the N$^{+453/30/88}$ strain led to new hydrophobic interactions between side chains of the 46th PR and 453rd p1/p6 residues, as well as of the PR 53F and p1/p6 P453L^{Gag} residues (Fig. 5C).

To examine whether these changes in interactions influenced the binding affinity of the p1/p6 substrate to PR, we analyzed

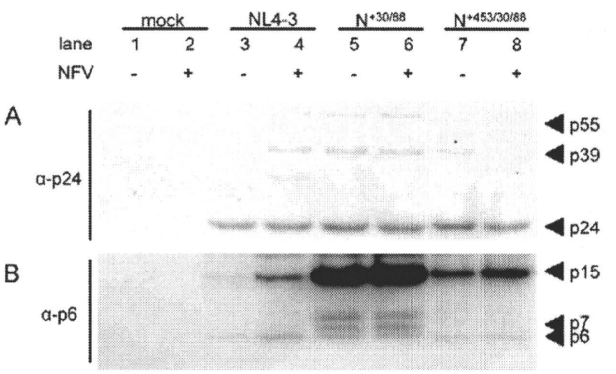

Fig. 4. Western blot analysis of Gag processing in the absence or presence of nelfinavir. Western blot analyses in the absence or presence of nelfinavir. HeLa cells were transfected by each recombinant clones and cultured in the absence or presence of NFV (0.1 μM). At 48 h post-transfection, virions in culture supernatants were harvested and subjected to Western blot analysis with anti-p24 monoclonal antibody (A) and an anti-p6 polyclonal antibody (B). Each lane was normalized by p24 antigen content (5 ng for each lane as determined by ELISA). Lanes 1 and 2, mock, lanes 3 and 4, NL4-3, lanes 5 and 6, N$^{+453/30/88}$, lanes 7 and 8, N$^{+30/88}$.

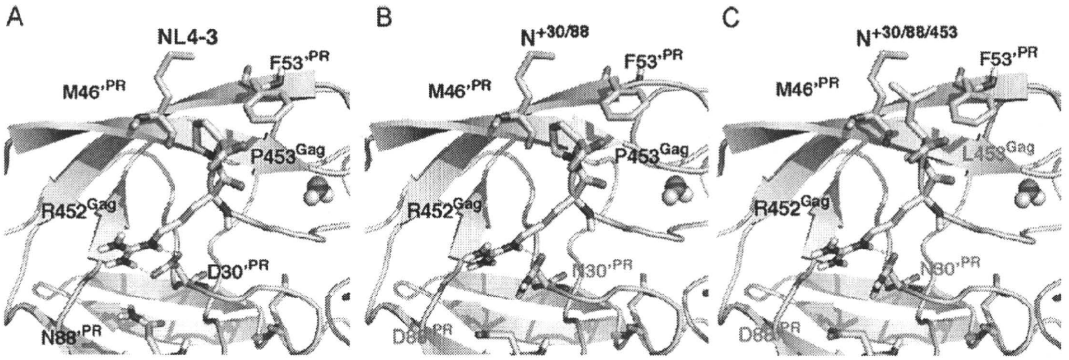

Fig. 5. Structural models of the Gag–PR complexes. Catalytic sites of the NL4-3 (A), $N^{+30/88}$ models (B), and $N^{+453/30/88}$ models (C) are highlighted. Green cartoons and sticks represent main and side chains of PR, respectively. Cyan sticks represent 452nd and 453rd residues in Gag corresponding to the p1/p6 region. (For interpretation of the references to color in this figure legend, the reader is referred to the web version of the article.)

their binding energies using the PR–p1/p6 peptide complex models. The predicted binding energies of the NL4-3, $N^{+30/88}$ and $N^{+453/30/88}$ models were −137.6 kcal/mol, −133.3 kcal/mol, and −137.1 kcal/mol, respectively, suggesting that p1/p6 substrate has lower affinity with $N^{+30/88}$ PR than with NL4-3 and $N^{+453/30/88}$ PRs. Taken together, these data suggest that PR mutations in the $N^{+30/88}$ strain can reduce Gag–PR affinity primarily via loss of the hydrogen bond between $N30^{PR}$ and $R452^{Gag}$ and that the Gag p1/p6 mutation in the $N^{+453/30/88}$ strain ($P453L^{Gag}$) can recover affinity by generating new hydrophobic interactions of $L453^{Gag}$ with $M46^{PR}$ and $F53^{PR}$.

3.7. $P453L^{Gag}/D30N^{PR}/N88D^{PR}$ association is commonly observed in a large database

To confirm the prevalence of the $P453L^{Gag}/D30N^{PR}/N88D^{PR}$ association in other HIV-infected individuals, we investigated 3249 sequences of HIV-1 subtype B *gag*-PR-coding region from the Los Alamos National Laboratory HIV sequence database (http://www.hiv.lanl.gov/). We found that the $P453L^{Gag}$ mutation was significantly associated with $D30N^{PR}/N88D^{PR}$ (Table 4; $p < 0.001$, Fisher's exact test). These data support the virological advantage of the $P453L^{Gag}/D30N^{PR}/N88D^{PR}$ association.

4. Discussion

In this study, we analyzed mechanisms of anti-HIV drug-resistant mutation acquisition by investigating crosstalk between Gag and PR mutations. We traced the clinical course and sequence changes in *gag* and the PR-coding region of a virological-failure case heavily treated with multiple regimens, including different protease inhibitors. To focus on the quality of sequence data and accuracy of analysis, we used SGS and Spidermonkey analysis, respectively.

Among the ten co-evolving Gag–Protease pairs inferred by Spidermonkey analysis, we confirmed a linkage between $P453L^{Gag}$ and $D30N^{PR}/N88D^{PR}$. $D30N^{PR}$ has been reported to associate with $N88D^{PR}$ (Rhee et al., 2007; Wu et al., 2003), P453L (Verheyen et al., 2006), and positively correlate with p1/p6 cleavage-site mutations (Kolli et al., 2006). We were interested in the association between $P453L^{Gag}$ and $D30N^{PR}/N88D^{PR}$ nelfinavir-resistant mutations, as $P453L^{Gag}$ is located at the P5′ position of the p1/p6 cleavage site, and expected to physically interact with the protease. Thus, we sought to clarify the biological advantage of interference among $P453L^{Gag}$, $D30N^{PR}$, and $N88D^{PR}$ in recombinant viruses with patient- and NL4-3-derived genetic backgrounds. Virological advantage was evaluated in three aspects: (1) virological superiority in replication competency, (2) resistance to antiretroviral selective pressure, and (3) Gag processing pattern in virions. Our results indicated that the $P453L^{Gag}$ cleavage-site mutation has the potential to improve the replication capacity and Gag processing of viruses with $D30N^{PR}/N88D^{PR}$, but has little effect on nelfinavir susceptibility. This latter finding is of interest since Gag cleavage-site mutations have been suggested as a mechanism for protease to develop drug resistance (Dam et al., 2009; Kolli et al., 2009). We also need to consider not only antiretroviral selective pressure but also immune selective pressure. Several of the positions we noted have been described as associated with human leukocyte antigen (HLA) escape mutations. For example, PR codons 12, 35, and 36, and Gag codons 373 and 374 are all potentially HLA-related (Brumme et al., 2009). To confirm the contributions of HLA and immune pressure, further study is required.

Although samples were collected chronologically at multiple times, the order of $P453L^{Gag}$, $D30N^{PR}$ and $N88D^{PR}$ acquisitions was unclear as all three mutations were detected at the same time. However, a plausible order seems to be the selection of $D30N^{PR}/N88D^{PR}$ followed by $P453L^{Gag}$ acquisition. Nelfinavir appears to select $D30N^{PR}/N88D^{PR}$ mutations for resistance because these mutations obviously increase drug resistance to nelfinavir (Johnson et al., 2009), whereas the $P453L^{Gag}$ mutation without any PR mutations has been reported to have almost no effect on susceptibility to PIs and on viral replication capacity (Maguire et al., 2002). Although $D30N^{PR}$ is known as one of the most unstable PI-resistant mutations (Martinez-Picado et al., 1999) and viruses with this mutation have lower PR activity than the wild-type, the impaired replication caused by $D30N^{PR}$ has been reported to be compensated by $N88D^{PR}$ (Mitsuya et al., 2006; Sugiura et al., 2002). Furthermore, the fitness of virus with $D30N^{PR}/N88D^{PR}$ was recovered in our study by an additional $P453L^{Gag}$ mutation (Fig. 3). However, the $P453L^{Gag}$ mutation was not introduced into NL4-3 carrying $D30N^{PR}/N88D^{PR}$ ($N^{+30/88}$) and patient $D30N^{PR}/N88D^{PR}$ clones (P^{-P453L}) during *in vitro* culture with nelfinavir, suggesting that the $P453L^{Gag}$ mutation is a sufficient condition for D30N/N88D clones to replicate efficiently.

Virus with $D30N^{PR}/N88D^{PR}$ was suggested by results of our Western blot analyses to process p1/p6 cleavage inefficiently, as

Table 4
Los Alamos National Laboratory HIV sequence database analysis.

453^{Gag}	$30^{PR}/88^{PR}$	
	D30/N88	N30N/D88D
P ($n = 2801$)	$n = 2743$	$n = 8$
L ($n = 237$)	$n = 223$	$n = 8$
p-value		<0.001

demonstrated by the accumulation of p15 and p7 non-cleaved precursors, but addition of P453L^{Gag} improved the processing (Fig. 4B). Accumulation of p15 and p7 products has been reported in previous studies using different PR mutant viruses (Doyon et al., 1996; Maguire et al., 2002). In these studies, the additional mutations at NC/p1 or p1/p6 cleavage sites also resulted in efficient processing of these precursors. Interestingly, an aberrant band, which did not match either p6 or p7, was observed in N$^{+30/88}$ in our study (Fig. 4, lanes 5 and 6). Although further analyses will be required to determine the exact mechanisms, the band suggests inaccurate or alternative recognition of the cleavage site by virus with D30N^{PR}/N88D^{PR}, and P453L^{Gag} may confer an advantage by adjusting the protease to recognize and cleave the right site. As the HIV-1 p6 protein is important for efficient particle budding (von Schwedler et al., 2003), the defect in p1/p6 cleavage may affect viral maturation, which in turn may reduce viral infectivity and replication capacity.

To understand the relevance of P453L^{Gag} from a structural viewpoint, we used homology modeling with the published X-ray crystal structure of the PR–p1/p6 substrate complex as a template (Fig. 5). Although P453L^{Gag} is located at the P5′ position and does not directly interfere with the protease active site or subsites, the modeling demonstrated that P453L^{Gag} can compensate for the binding affinity of PR and p1/p6. This mechanism is interesting because it suggests that a mutation outside the cleavage site interferes with the PR–Gag interaction. Indeed, Prabu-Jeyabalan et al. (2004) documented that a Gag mutation (A431V^{Gag}) compensates for a PR mutation (V82A^{PR}), which is not in direct contact with A431V^{Gag}. Thus, our data confirm the virological and structural advantages of P453L^{Gag} in viruses possessing D30N^{PR}/N88D^{PR}. Furthermore, this association appeared to be quite common as the frequency of P453L^{Gag} is 7.3% in the Los Alamos National Laboratory HIV sequence database. Though nelfinavir is no longer recommended as a first-line antiretroviral in the guidelines of developed countries, many cases previously exposed to nelfinavir have acquired D30N/N88D mutations. Indeed, the prevalence of the D30N mutation in PI-treated persons infected with subtype B viruses ($n = 7396$) and in nelfinavir-treated persons ($n = 1128$) is 7.9% and 28.1%, respectively, in the Stanford HIV drug resistance database (http://hivdb.stanford.edu/).

Regarding the bioinformatics analysis strategy, we selected the within-host substitution model in Spidermonkey analysis to infer the co-evolving sites (Nickle et al., 2007) as the data were sequences serially collected over 5 years from a single patient under anti-HIV treatment. One disadvantage of this program is that it does not account for the number of descendant clones. Often, mutation pairs on few viral clones might be determined as co-evolving pairs. In our study, 46^{PR} and 35^{PR} mutations were determined as a co-evolving pair with high posterior probability, but only one clone with this pair was observed among 129 sequences (Table 2), suggesting this co-mutation pair could not become "fixed" in a viral population. Thus, it is important to confirm the significance of the program output.

5. Conclusions

In conclusion, we successfully determined the Gag-protease associated sites P453L^{Gag}/D30N^{PR}/N88D^{PR} by applying single-genome sequencing, suggesting the usefulness of this method. However, as SGS is a more expensive method than direct sequencing, researchers need to consider which method has the best advantage for their samples. Extrapolating from our data, the relationships between the major mutations found by SGS may not differ significantly from direct sequencing results, but we might have a greater chance of seeing a variety of minority clones with minor mutations. In addition, our observation of higher variation at later sampling points suggests that cases with longer treatment histories are good sample candidates.

We found that the viruses acquiring P453L^{Gag}/D30N^{PR}/N88D^{PR} distinctly showed biological advantages. From results obtained using both viral experiments and bioinformatics, we speculate that the P453L^{Gag} mutation does not necessarily occur in the presence of nelfinavir, but if it occurs with D30N^{PR}/N88D^{PR} mutations, viral fitness can be improved, which may eventually lead to worse clinical outcomes of anti-HIV therapy. We believe that the findings of this study provide new insight into the mechanism of within-patient HIV-1 co-evolution and into the acquisition of resistance to anti-HIV drugs.

Acknowledgements

The authors thank Dr. Akira Shirahata and Mr. Yuki Kitamura for their support. We thank patients who contributed to our study. We also thank Ms. Claire Baldwin for her help in preparing the manuscript. This study was supported by a Grant-in-Aid for AIDS research from the Ministry of Health, Labor and Welfare of Japan (H19-AIDS-007), and also by Scientific Research from the Ministry of Education, Culture, Sports, and Technology of Japan (Project number: 19510208).

References

Altschuh, D., Lesk, A.M., Bloomer, A.C., Klug, A., 1987. Correlation of co-ordinated amino acid substitutions with function in viruses related to tobacco mosaic virus. J. Mol. Biol. 193, 693–707.

Baker, D., Sali, A., 2001. Protein structure prediction and structural genomics. Science 294, 93–96.

Bally, F., Martinez, R., Peters, S., Sudre, P., Telenti, A., 2000. Polymorphism of HIV type 1 gag p7/p1 and p1/p6 cleavage sites: clinical significance and implications for resistance to protease inhibitors. AIDS Res. Hum. Retroviruses 16, 1209–1213.

Bhattacharya, T., Daniels, M., Heckerman, D., Foley, B., Frahm, N., Kadie, C., Carlson, J., Yusim, K., McMahon, B., Gaschen, B., Mallal, S., Mullins, J.I., Nickle, D.C., Herbeck, J., Rousseau, C., Learn, G.H., Miura, T., Brander, C., Walker, B., Korber, B., 2007. Founder effects in the assessment of HIV polymorphisms and HLA allele associations. Science 315, 1583–1586.

Brumme, Z.L., John, M., Carlson, J.M., Brumme, C.J., Chan, D., Brockman, M.A., Swenson, L.C., Tao, I., Szeto, S., Rosato, P., Sela, J., Kadie, C.M., Frahm, N., Brander, C., Haas, D.W., Riddler, S.A., Haubrich, R., Walker, B.D., Harrigan, P.R., Heckerman, D., Mallal, S., 2009. HLA-associated immune escape pathways in HIV-1 subtype B Gag, Pol and Nef proteins. PLoS One 4, e6687.

Chiba-Mizutani, T., Miura, H., Matsuda, M., Matsuda, Z., Yokomaku, Y., Miyauchi, K., Nishizawa, M., Yamamoto, N., Sugiura, W., 2007. Use of new T-cell-based cell lines expressing two luciferase reporters for accurately evaluating susceptibility to anti-human immunodeficiency virus type 1 drugs. J. Clin. Microbiol. 45, 477–487.

Dam, E., Quercia, R., Glass, B., Descamps, D., Launay, O., Duval, X., Krausslich, H.G., Hance, A.J., Clavel, F., 2009. Gag mutations strongly contribute to HIV-1 resistance to protease inhibitors in highly drug-experienced patients besides compensating for fitness loss. PLoS Pathog. 5, e1000345.

Doyon, L., Croteau, G., Thibeault, D., Poulin, F., Pilote, L., Lamarre, D., 1996. Second locus involved in human immunodeficiency virus type 1 resistance to protease inhibitors. J. Virol. 70, 3763–3769.

Dutheil, J., Pupko, T., Jean-Marie, A., Galtier, N., 2005. A model-based approach for detecting coevolving positions in a molecule. Mol. Biol. Evol. 22, 1919–1928.

Gallego, O., de Mendoza, C., Corral, A., Soriano, V., 2003. Changes in the human immunodeficiency virus p7-p1-p6 gag gene in drug-naive and pretreated patients. J. Clin. Microbiol. 41, 1245–1247.

Gunthard, H.F., Wong, J.K., Ignacio, C.C., Havlir, D.V., Richman, D.D., 1998. Comparative performance of high-density oligonucleotide sequencing and dideoxynucleotide sequencing of HIV type 1 pol from clinical samples. AIDS Res. Hum. Retroviruses 14, 869–876.

Gutell, R.R., Power, A., Hertz, G.Z., Putz, E.J., Stormo, G.D., 1992. Identifying constraints on the higher-order structure of RNA: continued development and application of comparative sequence analysis methods. Nucleic Acids Res. 20, 5785–5795.

Hance, A.J., Lemiale, V., Izopet, J., Lecossier, D., Joly, V., Massip, P., Mammano, F., Descamps, D., Brun-Vézinet, F., Clavel, F., 2001. Changes in human immunodeficiency virus type 1 populations after treatment interruption in patients failing antiretroviral therapy. J. Virol. 75, 6410–6417.

Ho, S.K., Coman, R.M., Bunger, J.C., Rose, S.L., O'Brien, P., Munoz, I., Dunn, B.M., Sleasman, J.W., Goodenow, M.M., 2008. Drug-associated changes in amino acid residues in Gag p2, p7(NC), and p6(Gag)/p6(Pol) in human immunodeficiency virus type 1 (HIV-1) display a dominant effect on replicative fitness and drug response. Virology.

Johnson, V.A., Brun-Vézinet, F., Clotet, B., Gunthard, H.F., Kuritzkes, D.R., Pillay, D., Schapiro, J.M., Richman, D.D., 2008. Update of the drug resistance mutations in HIV-1: Spring 2008. Top. HIV Med. 16, 62–68.

Johnson, V.A., Brun-Vézinet, F., Clotet, B., Gunthard, H.F., Kuritzkes, D.R., Pillay, D., Schapiro, J.M., Richman, D.D., 2009. Update of the drug resistance mutations in HIV-1: December 2009. Top. HIV Med. 17, 138–145.

Koch, N., Yahi, N., Fantini, J., Tamalet, C., 2001. Mutations in HIV-1 gag cleavage sites and their association with protease mutations. AIDS 15, 526–528.

Kolli, M., Lastere, S., Schiffer, C.A., 2006. Co-evolution of nelfinavir-resistant HIV-1 protease and the p1-p6 substrate. Virology 347, 405–409.

Kolli, M., Stawiski, E., Chappey, C., Schiffer, C.A., 2009. Human immunodeficiency virus type 1 protease-correlated cleavage site mutations enhance inhibitor resistance. J. Virol. 83, 11027–11042.

Labute, P., 2008. The generalized Born/volume integral implicit solvent model: estimation of the free energy of hydration using London dispersion instead of atomic surface area. J. Comput. Chem. 29, 1693–1698.

Maguire, M.F., Guinea, R., Griffin, P., Macmanus, S., Elston, R.C., Wolfram, J., Richards, N., Hanlon, M.H., Porter, D.J., Wrin, T., Parkin, N., Tisdale, M., Furfine, E., Petropoulos, C., Snowden, B.W., Kleim, J.P., 2002. Changes in human immunodeficiency virus type 1 Gag at positions L449 and P453 are linked to I50V protease mutants in vivo and cause reduction of sensitivity to amprenavir and improved viral fitness in vitro. J. Virol. 76, 7398–7406.

Mahalingam, B., Louis, J.M., Reed, C.C., Adomat, J.M., Krouse, J., Wang, Y.F., Harrison, R.W., Weber, I.T., 1999. Structural and kinetic analysis of drug resistant mutants of HIV-1 protease. Eur. J. Biochem. 263, 238–245.

Malet, I., Roquebert, B., Dalban, C., Wirden, M., Amellal, B., Agher, R., Simon, A., Katlama, C., Costagliola, D., Calvez, V., Marcelin, A.G., 2007. Association of Gag cleavage sites to protease mutations and to virological response in HIV-1 treated patients. J. Infect. 54, 367–374.

Marti-Renom, M.A., Stuart, A.C., Fiser, A., Sanchez, R., Melo, F., Sali, A., 2000. Comparative protein structure modeling of genes and genomes. Annu. Rev. Biophys. Biomol. Struct. 29, 291–325.

Martin, L.C., Gloor, G.B., Dunn, S.D., Wahl, L.M., 2005. Using information theory to search for co-evolving residues in proteins. Bioinformatics 21, 4116–4124.

Martinez-Picado, J., Savara, A.V., Sutton, L., D'Aquila, R.T., 1999. Replicative fitness of protease inhibitor-resistant mutants of human immunodeficiency virus type 1. J. Virol. 73, 3744–3752.

Matsuoka-Aizawa, S., Sato, H., Hachiya, A., Tsuchiya, K., Takebe, Y., Gatanaga, H., Kimura, S., Oka, S., 2003. Isolation and molecular characterization of a nelfinavir (NFV)-resistant human immunodeficiency virus type 1 that exhibits NFV-dependent enhancement of replication. J. Virol. 77, 318–327.

Meyerhans, A., Vartanian, J.P., Wain-Hobson, S., 1990. DNA recombination during PCR. Nucleic Acids Res. 18, 1687–1691.

Mitsuya, Y., Winters, M.A., Fessel, W.J., Rhee, S.Y., Hurley, L., Horberg, M., Schiffer, C.A., Zolopa, A.R., Shafer, R.W., 2006. N88D facilitates the co-occurrence of D30N and L90M and the development of multidrug resistance in HIV type 1 protease following nelfinavir treatment failure. AIDS Res. Hum. Retroviruses 22, 1300–1305.

Myint, L., Matsuda, M., Matsuda, Z., Yokomaku, Y., Chiba, T., Okano, A., Yamada, K., Sugiura, W., 2004. Gag non-cleavage site mutations contribute to full recovery of viral fitness in protease inhibitor-resistant human immunodeficiency virus type 1. Antimicrob. Agents Chemother. 48, 444–452.

Neher, E., 1994. How frequent are correlated changes in families of protein sequences? Proc. Natl. Acad. Sci. U. S. A. 91, 98–102.

Nickle, D.C., Heath, L., Jensen, M.A., Gilbert, P.B., Mullins, J.I., Kosakovsky Pond, S.L., 2007. HIV-specific probabilistic models of protein evolution. PLoS One 2, e503.

Nijhuis, M., Schuurman, R., de Jong, D., Erickson, J., Gustchina, E., Albert, J., Schipper, P., Gulnik, S., Boucher, C.A., 1999. Increased fitness of drug resistant HIV-1 protease as a result of acquisition of compensatory mutations during suboptimal therapy. AIDS 13, 2349–2359.

Palmer, S., Kearney, M., Maldarelli, F., Halvas, E.K., Bixby, C.J., Bazmi, H., Rock, D., Falloon, J., Davey Jr., R.T., Dewar, R.L., Metcalf, J.A., Hammer, S., Mellors, J.W., Coffin, J.M., 2005. Multiple, linked human immunodeficiency virus type 1 drug resistance mutations in treatment-experienced patients are missed by standard genotype analysis. J. Clin. Microbiol. 43, 406–413.

Pollock, D.D., Taylor, W.R., 1997. Effectiveness of correlation analysis in identifying protein residues undergoing correlated evolution. Protein Eng. 10, 647–657.

Poon, A.F., Kosakovsky Pond, S.L., Richman, D.D., Frost, S.D., 2007a. Mapping protease inhibitor resistance to human immunodeficiency virus type 1 sequence polymorphisms within patients. J. Virol. 81, 13598–13607.

Poon, A.F., Lewis, F.I., Frost, S.D., Pond, S.L., 2008. Spidermonkey: rapid detection of co-evolving sites using Bayesian graphical models. Bioinformatics.

Poon, A.F., Lewis, F.I., Pond, S.L., Frost, S.D., 2007b. An evolutionary-network model reveals stratified interactions in the V3 loop of the HIV-1 envelope. PLoS Comput. Biol. 3, e231.

Prabu-Jeyabalan, M., Nalivaika, E., Schiffer, C.A., 2002. Substrate shape determines specificity of recognition for HIV-1 protease: analysis of crystal structures of six substrate complexes. Structure 10, 369–381.

Prabu-Jeyabalan, M., Nalivaika, E.A., King, N.M., Schiffer, C.A., 2004. Structural basis for coevolution of a human immunodeficiency virus type 1 nucleocapsid-p1 cleavage site with a V82A drug-resistant mutation in viral protease. J Virol 78, 12446–12454.

Rhee, S.Y., Liu, T.F., Holmes, S.P., Shafer, R.W., 2007. HIV-1 subtype B protease and reverse transcriptase amino acid covariation. PLoS Comput. Biol. 3, e87.

Saitou, N., Nei, M., 1987. The neighbor-joining method: a new method for reconstructing phylogenetic trees. Mol. Biol. Evol. 4, 406–425.

Sayer, J.M., Liu, F., Ishima, R., Weber, I.T., Louis, J.M., 2008. Effect of the active site D25N mutation on the structure, stability, and ligand binding of the mature HIV-1 protease. J. Biol. Chem. 283, 13459–13470.

Shirakawa, K., Takaori-Kondo, A., Yokoyama, M., Izumi, T., Matsui, M., Io, K., Sato, T., Sato, H., Uchiyama, T., 2008. Phosphorylation of APOBEC3G by protein kinase A regulates its interaction with HIV-1 Vif. Nat. Struct. Mol. Biol. 15, 1184–1191.

Sugiura, W., Matsuda, Z., Yokomaku, Y., Hertogs, K., Larder, B., Oishi, T., Okano, A., Shiino, T., Tatsumi, M., Matsuda, M., Abumi, H., Takata, N., Shirahata, S., Yamada, K., Yoshikura, H., Nagai, Y., 2002. Interference between D30N and L90M in selection and development of protease inhibitor-resistant human immunodeficiency virus type 1. Antimicrob. Agents Chemother. 46, 708–715.

Tillier, E.R., Lui, T.W., 2003. Using multiple interdependency to separate functional from phylogenetic correlations in protein alignments. Bioinformatics 19, 750–755.

Tuff, P., Darlu, P., 2000. Exploring a phylogenetic approach for the detection of correlated substitutions in proteins. Mol. Biol. Evol. 17, 1753–1759.

Verheyen, J., Litau, E., Sing, T., Daumer, M., Balduin, M., Oette, M., Fatkenheuer, G., Rockstroh, J.K., Schuldenzucker, U., Hoffmann, D., Pfister, H., Kaiser, R., 2006. Compensatory mutations at the HIV cleavage sites p7/p1 and p1/p6-gag in therapy-naive and therapy-experienced patients. Antivir. Ther. 11, 879–887.

von Schwedler, U.K., Stuchell, M., Muller, B., Ward, D.M., Chung, H.Y., Morita, E., Wang, H.E., Davis, T., He, G.P., Cimbora, D.M., Scott, A., Krausslich, H.G., Kaplan, J., Morham, S.G., Sundquist, W.I., 2003. The protein network of HIV budding. Cell 114, 701–713.

Wang, J., Cieplak, P., Kollman, P.A., 2000. How well does a restrained electrostatic potential (RESP) model perform in calculating conformational energies of organic and biological molecules? Journal of Computational Chemistry 21, 1049–1074.

Willey, R.L., Smith, D.H., Lasky, L.A., Theodore, T.S., Earl, P.L., Moss, B., Capon, D.J., Martin, M.A., 1988. In vitro mutagenesis identifies a region within the envelope gene of the human immunodeficiency virus that is critical for infectivity. J. Virol. 62, 139–147.

Wollenberg, K.R., Atchley, W.R., 2000. Separation of phylogenetic and functional associations in biological sequences by using the parametric bootstrap. Proc. Natl. Acad. Sci. U. S. A. 97, 3288–3291.

Wu, T.D., Schiffer, C.A., Gonzales, M.J., Taylor, J., Kantor, R., Chou, S., Israelski, D., Zolopa, A.R., Fessel, W.J., Shafer, R.W., 2003. Mutation patterns and structural correlates in human immunodeficiency virus type 1 protease following different protease inhibitor treatments. J. Virol. 77, 4836–4847.

Yeang, C.H., Haussler, D., 2007. Detecting coevolution in and among protein domains. PLoS Comput. Biol. 3, e211.

Zhang, Y.M., Imamichi, H., Imamichi, T., Lane, H.C., Falloon, J., Vasudevachari, M.B., Salzman, N.P., 1997. Drug resistance during indinavir therapy is caused by mutations in the protease gene and in its Gag substrate cleavage sites. J. Virol. 71, 6662–6670.

JOURNAL OF CLINICAL MICROBIOLOGY, Mar. 2011, p. 1017–1024 Vol. 49, No. 3
0095-1137/11/$12.00 doi:10.1128/JCM.02149-10

Outbreak of Infections by Hepatitis B Virus Genotype A and Transmission of Genetic Drug Resistance in Patients Coinfected with HIV-1 in Japan▽

Seiichiro Fujisaki,[1] Yoshiyuki Yokomaku,[1] Teiichiro Shiino,[2] Tomohiko Koibuchi,[3] Junko Hattori,[1] Shiro Ibe,[1] Yasumasa Iwatani,[1,4] Aikichi Iwamoto,[3] Takuma Shirasaka,[5] Motohiro Hamaguchi,[6] and Wataru Sugiura[1,4]*

Department of Infectious Diseases and Immunology, Clinical Research Center, National Hospital Organization, Nagoya Medical Center, Nagoya, Japan[1]; Infectious Disease Surveillance Center, National Institute of Infectious Diseases, Tokyo, Japan[2]; Institute of Medical Science, The University of Tokyo, Tokyo, Japan[3]; Department of AIDS Research, Nagoya University Graduate School of Medicine, Nagoya, Japan[4]; AIDS Medical Center, National Hospital Organization, Osaka National Hospital, Osaka, Japan[5]; and Aichi Blood Center, Japanese Red Cross Society, Nagoya, Japan[6]

Received 24 October 2010/Returned for modification 2 December 2010/Accepted 8 January 2011

The major routes of hepatitis B virus (HBV) infection in Japan has been mother-to-child transmission (MTCT) and blood transfusion. However, HBV cases transmitted through sexual contact are increasing, especially among HIV-1-seropositive patients. To understand the molecular epidemiology of HBV in HBV/HIV-1 coinfection, we analyzed HBV genotypes and HIV-1 subtypes in HBV/HIV-1-coinfected patients at Nagoya Medical Center from 2003 to 2007. Among 394 HIV-1-infected Japanese men having sex with men (MSM) who were newly diagnosed during the study period, 31 (7.9%) tested positive for the hepatitis B virus surface antigen. HBV sequence analyses were successful in 26 cases, with 21 (80.7%) and 5 (19.3%) cases determined as genotypes A and C, respectively. Our finding that HBV genotype A was dominant in HIV-1-seropositive patients alerts clinicians to an alternative outbreak of HBV genotype A in the HIV-1-infected MSM population and a shift in HBV genotype from C to A in Japan. The narrow genetic diversity in genotype A cases suggests that genotype A has been recently introduced into the MSM population and that sexual contacts among MSM were more active than speculated from HIV-1 tree analyses. In addition, we found a lamivudine resistance mutation in one naïve case, suggesting a risk of drug-resistant HBV transmission. As genotype A infection has a higher risk than infection with other genotypes for individuals to become HBV carriers, prevention programs are urgently needed for the target population.

The number of hepatitis B virus (HBV)-infected persons in Japan is estimated to be 1 million, or 0.8% of the total population (31). HBV is classified into eight genotypes, A to H, by their differences in genome sequences (11, 12, 22). Circulating genotypes in Japan differ according to geographical region, with the prevalent genotypes in 2001 being C (84.7%) and B (12.2%), while A (1.7%) and D (0.4%) were less frequent (17). HBV infection in Japan has been transmitted mainly by two routes, mother-to-child transmission (MTCT) and blood transfusion, which have been targeted by prevention programs still being operated today (13, 15–17, 25).

Regarding MTCT, all pregnant women are screened for HBV antigen and antibody. Mothers who are HBV infected are prohibited from breast-feeding, and their newborns are vaccinated against HBV. Regarding infection by blood transfusion, all donated blood is tested by anti-hepatitis B surface antibody (HBsAb) testing and PCR to exclude HBV-contaminated blood from the supply. These prevention programs have been successful, and the risks of HBV infection by these two routes have been reduced dramatically.

However, HBV infection by sexual contact has recently become a prevailing alternative transmission route of HBV in Japan (30, 36). In particular, coinfection with HBV and human immunodeficiency virus type 1 (HIV-1), the causative agent of AIDS, has been increasing among men who have sex with men (MSM), and the incidence of HBV infection associated with HIV-1-seropositive cases appeared to be 8.8%, which is higher than that in the general population (5). Thus, the epidemiology of HBV infection in Japan is quickly shifting. Here we report the most recent molecular epidemiologic status of HBV/HIV-1 coinfection.

MATERIALS AND METHODS

Sample. HIV/AIDS patients newly diagnosed at Nagoya Medical Center from 2003 to 2007 were tested for hepatitis B surface antigen (HBsAg), and HBsAg-positive patients were enrolled in the study. Clinical data (age, gender, suspected route of HIV-1 infection, aspartate aminotransferase [AST] and alanine aminotransferase [ALT] plasma levels, CD4-positive T cell count, and HIV viral load) were obtained from medical records. Plasma HBV viral load was measured with COBAS TaqMan (Roche Diagnostics, Basel, Switzerland), and plasma HBc IgM titer was measured with Lumipulse (Fujirebio, Tokyo, Japan). The time of HBV infection was estimated by patient interview and HBc IgM titer results. This study was conducted according to the principles expressed in the Declaration of Helsinki. The study was approved by the Institutional Review Boards of the National Institute of Infectious Diseases and Nagoya Medical Center. All pa-

* Corresponding author. Mailing address: Department of Infection and Immunology, Clinical Research Center, Nagoya Medical Center, 4-1-1 Sannomaru, Nakaku, Nagoya 4600001, Japan. Phone: 81-52-951-1111. Fax: 81-52-963-3970. E-mail: wsugiura@nnh.hosp.go.jp.

▽ Published ahead of print on 19 January 2011.

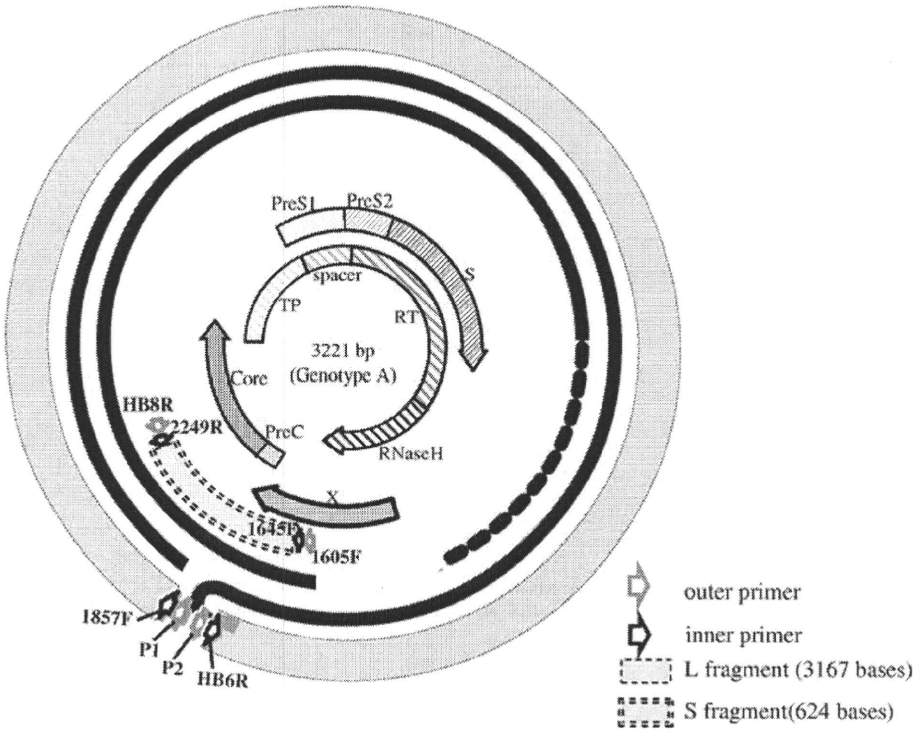

FIG. 1. Genetic regions of HBV and HIV-1 used for phylogenetic tree analyses. The whole HBV genome was amplified in two fragments, L and S, and assembled. L and S fragments are indicated by single and double dashed lines, respectively.

tients provided written informed consent for collection of samples and subsequent analysis.

Amplification of HBV and HIV DNA fragments and determination of DNA sequences. HBV nucleic acid was extracted from plasma using a MagNA Pure Compact Nucleic Acid Isolation Kit I (Roche Diagnostics). As shown in Fig. 1, the full-length HBV genome was amplified in two fragments, L (3,167 bases) and S (624 bases). The primers used for amplifying HBV DNA were both newly designed and have been published previously (27). Details of these primers are summarized in Table 1. The DNA polymerases used for the first and nested PCRs were LA *Taq* (Takara, Shiga, Japan) and Prime Star HS (Takara) polymerase, respectively. The HBV genotypes were also determined using a commercial kit (Institute of Immunology, Tokyo, Japan) based on enzyme immunoassay to confirm that the results did not differ from those based on phylogenetic tree analysis.

The HIV-1 *gag p17* (396 bp [bp 790 to 1185]), *pol* (1,117 bp [bp 2253 to 3369]), and *env C2V3* (222 bp [bp 6996 to 7217]) regions were amplified from extracted plasma HIV-1 RNA by reverse transcription-PCR (RT-PCR) using the SuperScript one-step RT-PCR system for long templates (Invitrogen, Carlsbad, CA)

TABLE 1. Primers for amplifying the HBV and HIV-1 genomes

Name	Direction[a]	Sequence (5′ → 3′)	Region
P1	F	TTTTCACCTCTGCCTAATCA	First PCR, HBV L fragment
P2	R	AAAAAGTTGCATGGTGCTGG	First PCR, HBV L fragment
1605F	F	CGCATGGAGACCACCGTGAA	First PCR, HBV S fragment
HB8R	R	ATAGGGGCATTTGGTGGTCT	First PCR, HBV S fragment
1857F	F	CTACTGTTCAAGCCTCCAAG	Nested PCR, HBV L fragment
HB6R	R	AACAGACCAATTTATGCCTA	Nested PCR, HBV L fragment
1645F	R	AGGTCTTGCATAAGAGGACT	Nested PCR, HBV S fragment
2249R	F	CCAAAAGACACCAAATAYTC	Nested PCR, HBV S fragment
172A	F	ATCTCTAGCAGTGGCGCCCGAACAG	RT-PCR, HIV-1 *gag* fragment
173B	R	CTGATAATGCTGAAAACATGGGTAT	RT-PCR, HIV-1 *gag* fragment
174A	F	CTCTCGACGCAGGACTCGGCTTGCT	Nested PCR, HIV-1 *gag* fragment
175B	R	CCCATGCATTCAAAGTTCTAGGTGA	Nested PCR, HIV-1 *gag* fragment
K1	F	AAGGGCTGTTGGAAATGTGG	RT-PCR, HIV-1 *pol* fragment
U13	R	CCCACTCAGGAATCCAGGT	RT-PCR, HIV-1 *pol* fragment
K4	F	GAAAGGAAGGACACCAAATGA	nested PCR, HIV-1 *pol* fragment
U12	R	CTCATTCTTGCATATTTTCCTGTT	Nested PCR, HIV-1 *pol* fragment
106A	F	CATACATTATTGTGCCCCGGCTGG	RT-PCR, HIV-1 *env* fragment
17B	R	AGAAAAATTCCCCTCTACAATTAA	RT-PCR, HIV-1 *env* fragment
14A	F	AATGTCAGCTCAGTACAATGCACAC	Nested PCR, HIV-1 *env* fragment
10B	R	ATTTCTGGGTCCCCTCCTGAGG	Nested PCR, HIV-1 *env* fragment

[a] F, forward; R, reverse.

TABLE 2. HBV genotype reference sequences collected from the DNA Database of Japan (DDBJ) for tMRCA analysis

Genotype	DDBJ accession no.
A	FJ692588, GQ325786, GQ477503, GQ477496, GQ486599, EU414132
B	FJ751547, GQ924611
C	GQ924615, GQ486096, EU939589, GQ486684
D	GQ486337, FJ349228, GQ924652, EU414124, GQ922001, GQ486586
E	GQ486756, GQ161830, FJ349237
F	GQ486537, GQ486515, GQ486570
G	GQ486843
H	GQ486592, AB266536

followed by a second PCR using LA *Taq* polymerase. The primers used for HIV-1 sequencing are also summarized in Table 1. The amplicons were purified using a MultiScreen PCR filter plate (Millipore, Billerica, MA), and the sequencing reaction was performed using the BigDye Terminator v3.1 cycle sequencing kit (Applied Biosystems, Carlsbad, CA) and analyzed with the ABI PRISM 3130 (Applied Biosystems) autosequencer. Electropherograms were edited and verified by SeqScape v2.5 software (Applied Biosystems).

Phylogenetic tree analyses and genotype determination. HBV genotypes were determined by phylogenetic tree analysis with reference sequences. HBV sequences were aligned with 23 reference sequences from the National Center for Biotechnology Information (NCBI) database by using the CLUSTAL W program and analyzed by Kimura two-parameter methods. Genetic distances were calculated by the maximum composite likelihood, and phylogenetic trees were constructed by the neighbor-joining method using MEGA version 4 software. The reliabilities of branches were evaluated by bootstrap analysis with 1,000 replicates.

Phylogenetic trees of the HIV-1 *gag*, *pol*, and *env* regions were also constructed with 62 HIV-1 reference sequences obtained from the HIV-1 sequence database (Los Alamos National Laboratory).

Estimated tMRCAs. Evolutionary rates, chronological phylogenies, and other evolutionary parameters of HBV genotypes were estimated from heterochronous data for the HBV genomic sequences collected in our study, together with reference sequences from public databases (Table 2), using the Bayesian Markov chain Monte Carlo (MCMC) method. The nucleotide substitution model was evaluated by the hierarchical likelihood ratio test using PAUP v4.0 (29) with MrModeltest (14) and the general time-reversible (GTR) model with both invariant site (I) and gamma-distributed site (G) heterogeneity for four rate categories showing maximum likelihood. Bayesian MCMC analyses were performed with BEAST v1.4.8 (4) using the substitution model of GTR + I + G, three partitions into codon positions, and a relaxed molecular clock model (the uncorrelated log normal-distributed model) (3). Four different population dynamic models (exponential growth, logistic growth, constant population, and Bayesian skyline plot [BSP]) were tested in the analyses. According to BSP properties, constant-growth models were adopted for the HBV genome sequences. Each Bayesian MCMC analysis was run for 40 million states and sampled every 10,000 states. Posterior probabilities were calculated with a burn-in of 4 million states and checked for convergence using Tracer v1.4 (21). The maximum clade credibility tree for analyzing the MCMC data set was annotated by TreeAnnotator in the BEAST package. The posterior distribution of the substitution rate obtained from the heterochronous sequences was subsequently incorporated as a prior distribution for the mean evolutionary rate of the HBV genome, thereby adding a time scale to the phylogenetic histories of the given viruses and enabling estimation of the time of the most recent common ancestor (tMRCA) (19).

Determination of HBV drug resistance mutations. HBV cases resistant to nucleoside analogue reverse transcriptase inhibitors (NRTI) were determined by analyzing amino acid sequences of the RT region. The approved anti-HBV drugs in Japan are lamivudine, adefovir, and entecavir. In cases of HBV/HIV-1 coinfection, tenofovir and emtricitabine are also used. We studied whether the viruses have drug resistance mutations against these antiretroviral drugs with or without a history of antiretroviral treatments and confirmed the following resistance mutations: lamivudine/emtricitabine resistance mutations V173L, L180M, and M204I/V; adefovir resistance mutations A181V, I233V, and N236T; entecavir resistance mutations I169T, L180M, T184G, S202I, M204I/V, and M250V; and tenofovir resistance mutation A194T (1, 2, 24, 32, 34, 35). Furthermore, major drug resistance mutations in HIV-1 were defined according to the criteria of the International AIDS Society (IAS)-USA and Stanford HIV drug resistance database (7, 23).

RESULTS

The major HBV genotype circulating among Japanese MSM is genotype A. During the study period, 394 cases were newly diagnosed as HIV/AIDS, and 31 cases were determined as HBsAg positive. Thus, the average prevalence of HBV/HIV-1 coinfection in our study population was 7.9%. Analysis of the coinfection prevalence in each year showed increases from 2.8 to 3.3% in 2003 to 2004 and from 7.4 to 13.2% in 2005 to 2007 (Fig. 2). As the suspected route of HIV-1 infections in all 31 cases was MSM, HBV appears to be quickly spreading among the MSM population. Of these HBV/HIV-1-coinfected cases, 26 isolates were successfully sequenced for both HBV and HIV-1, and their subtypes and genotypes were determined. Regarding the five cases for which the HBV genome could not be sequenced, plasma HBV DNA copies were undetectable in four cases, and low ($10^{3.3}$ copies/ml) in one case.

The median age of the patients was 34 years (interquartile range [IQR], 29.5 to 37.0) (Table 3). The median plasma viral loads of HBV and HIV-1 were 4.4×10^8 (IQR, 4.9×10^4 – 6.3×10^8) and 6.4×10^4 (IQR, 2.0×10^4–2.0×10^5) copies/ml, respectively. Hepatitis B core antigen (HBcAg) IgM was positive in nine patients, of which two were suspected to harbor acute HBV infection according to their HBsAg positivity, AST and ALT plasma levels, and patient interviews. The other 7 HBcAg-positive patients were categorized as having acute hepatitis or exacerbated chronic hepatitis, and 17 HBcAg-negative patients were determined as being in the chronic hepatitis stage.

According to phylogenetic tree analysis, 26 cases were classified into two genotypes, either A or C. As shown in Fig. 3, 21 and 5 cases were classified as genotypes A and C, respectively. The subgenotypes of the 21 genotype A cases were all A2, the predominant subgenotype in Europe and North America, whereas the subgenotypes of the 5 genotype C cases were all C1, the most prevalent subgenotype in eastern Asia, including Japan, South Korea, and northern China. Genotype B, the

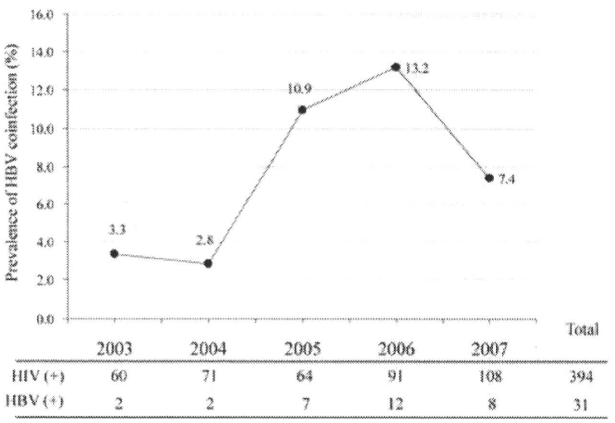

FIG. 2. Transitions in HBV infection rates in HBV/HIV-1-coinfected patients. HBV infection rates are plotted versus year, with the numbers of HIV-1-infected and HBV/HIV-1-coinfected patients shown below the *x* axis.

TABLE 3. Characteristics of HBV/HIV-1-coinfected patients

Characteristic	Value[a] for genotype:			*P*
	All (n = 26)	A (n = 21)	C (n = 5)	
Age (yr)	34 (30–37)	33 (29–37)	56 (46–57)	<0.01
Suspected route of HIV-1 infection	MSM	MSM	MSM	
AST (IU/liter)	31 (26–63)	29 (26–48)	54 (20–74)	
ALT (IU/liter)	43 (33–90)	42 (32–85)	44 (34–99)	
No. HBcAg IgM positive	9	9	0	<0.01
CD4 (/μl)	293 (91–492)	300 (94–484)	202 (9–494)	
HIV-1viral load (copies/ml)	6.4×10^4 (2.0×10^4–2.0×10^5)	6.8×10^4 (2.4×10^4–2.1×10^5)	2.4×10^4 (2.4×10^3–9.7×10^4)	
HBV viral load (copies/ml)	4.4×10^8 (4.9×10^4–6.3×10^8)	6.3×10^8 (4.7×10^4–6.3×10^8)	2.0×10^8 (4.7×10^5–6.3×10^8)	

[a] Median values are shown. Numbers in parentheses represent interquartile ranges.

second most predominant HBV genotype in Japan, was not detected in our study. Interestingly, the genotype A and C populations showed obvious differences in genetic diversity. The 21 group A2 samples (Fig. 3) formed a cluster with little

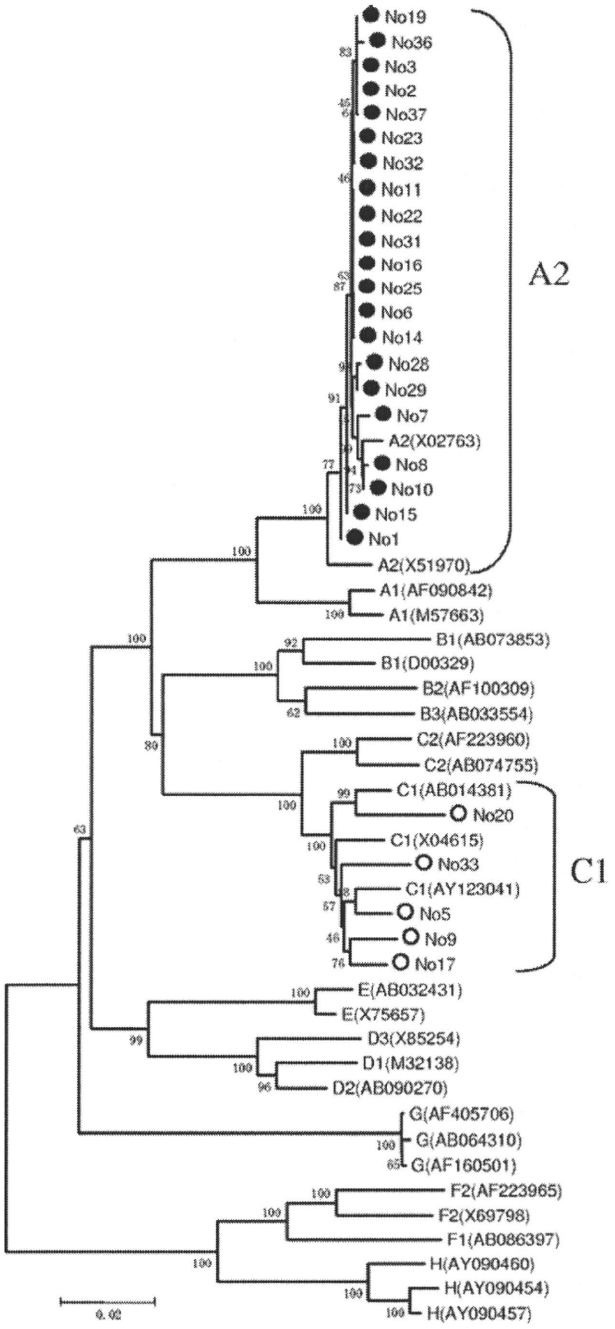

FIG. 3. Phylogenetic tree analyses of HBV isolated from HBV/HIV-1-coinfected patients. The phylogenetic tree was constructed using 26 full-length HBV genome sequences detected in HBV/HIV-1-coinfected patients in Nagoya (both solid and open circles) and 23 reference sequences from the NCBI database. Twenty-one and five cases were distributed in the clusters of genotype A (solid circles) and C (open circles), respectively.